

THE JOURNAL OF CHEMICAL PHYSICS

VOLUME 43, NUMBER 8

15 OCTOBER 1965

Discreteness-of-Charge Adsorption Micropotentials. II. Single Imaging

C. A. BARLOW, JR., AND J. R. MACDONALD
Texas Instruments Incorporated, Dallas, Texas
(Received 21 May 1965)

Methods are developed for calculating exact potentials and fields arising from discrete hexagonal arrays of monopoles imaged by a perfect conductor. They allow calculation of the potential and field at any point outside a plane electrode upon which such a hexagonal array of charges (of infinite extent) is adsorbed, and are applied to the problem of determining various electrical properties of such adsorbed arrays. We give particular attention to the micropotential and energy of adsorption for ionic adsorption in both electrolytic and gaseous systems and consider further application of the results to electron emission from metals. Detailed comparison with earlier approximate treatments is made, and when appropriate, errors appearing there are corrected. For example, we find that the rearrangement energy on incremental adsorption of ions does not vanish, as previously suggested, except for a nonphysical limit. Exact results are obtained for the rearrangement energy, and it is usually found to be a significant contribution to the total adsorption energy. Sufficient graphical and numerical results are given for all computed quantities so as to be of direct use to the worker in this general area.

INTRODUCTION

IN the first paper in this series,¹ we considered discreteness-of-charge effects in the infinite-imaging situation pertinent to ionic adsorption from an electrolyte onto a smooth, plane, conducting electrode. The discrete, adsorbed ions are assumed, because of mutual planar repulsion, to arrange themselves in a hexagonal array of spacing r_1 , as in Fig. 1(a), with the spacing dependent on the concentration of adsorbed ions. A glossary of important terms appears in the next section. In the infinite-imaging situation, the charges of the adsorbed ions are taken to be perfectly imaged in both the conducting electrode and in the outer Helmholtz plane (OHP), the plane of closest approach to the electrode of the charge centroids of unadsorbed ions in solution. Imaging in the OHP was assumed in I to arise from both the higher dielectric constant of water beyond the OHP than that between it and the electrode and from a high concentration of moveable ions at the OHP.

In a subsequent paper, we hope to treat the general situation of partial imaging at the OHP, probably that most appropriate for the electrolyte case, while continuing to assume perfect imaging in the electrode.

¹ C. A. Barlow, Jr., and J. R. Macdonald, *J. Chem. Phys.* **40**, 1535 (1964). In Eq. (23) of this paper, the term in the square bracket should be in the denominator, not the numerator, of the equation. This paper is referred to as I.

Here, we consider the opposite extreme to infinite imaging, the single-imaging case shown in Fig. 1(b) where all imaging at the OHP has been neglected. Although this situation is not likely to approximate the true state of affairs well in the electrolyte case except to some degree at low electrolyte concentrations and small ionic adsorption, it is most appropriate for adsorption of charged entities from a gas phase. Further, it is of interest to discover how much single-imaging results differ from infinite-imaging ones in the electrolyte situation in order to assess quantitatively how much total effect partial, rather than complete, imaging can produce. Should the single-imaging results be almost indistinguishable from the complete infinite-imaging ones, then it would not be worthwhile to carry out the more difficult partial-imaging analysis. Although there is an infinite number of images even in the partial-imaging case, for convenience we reserve the term "infinite imaging" for perfect imaging of charges between two conducting, parallel planes.

We shall be concerned with two distinct problems in the present single-imaging situation. The first, particularly appropriate for work-function and high-field-emission studies, is the calculation of the potential and the fields anywhere outside the adsorbing electrode when there is no vacant site and the hexagonal array of adions and the corresponding hexagonal image array are complete. We do not consider boundary effects and

hence restrict attention to maximum distances perpendicular to the array very large (to be approximated by "infinity") compared to array charge spacing but small compared to array planar extent. Of course, for distances very large compared to the maximum planar extent of the array, the potential and fields will be zero.

The second problem is the classical micropotential problem where one principally asks what is the work required to bring an ion from "infinity" or some smaller distance to a vacant adsorption site in the array. The work of redistribution required to form this vacancy from an initially complete array with slightly larger r_1 is considered later.

In treating the micropotential problem, we are primarily concerned with the potential and normal field along the line perpendicular to the plane electrode through the position of a vacant site in the array. The conventional micropotential, extensively used in the electrolyte case, is defined as the potential, taking discreteness of charge into account, at the site of the vacant ion ($z=\beta$), the inner Helmholtz plane (IHP), minus the corresponding potential at the OHP ($z=\beta+\gamma$), both calculated without including any contribution from the missing ion and its image in the electrode. The omission of the effect of the ion and its infinite line of images was a necessity in the infinite imaging case since, as pointed out in I, they lead to an infinite contribution to the micropotential. This is not the case in the present situation, and we later consider the effect of the addition of the ion and its single image to the actual potential, which should properly be used in the adsorption isotherm. As the ion is brought towards the vacant site as shown in Fig. 1(b), its image moves, and the charges of both the real ion and its image contribute to the work of adsorption; thus, their effects should properly be included in the adsorption isotherm. When adsorption from a gas phase is considered, there is no definable OHP, and we may introduce a near-field micropotential (NFM) as the difference between the potential (again neglecting the contribution of the ion and its image) at the IHP and that at "infinity." The latter quantity, $\psi_\infty \equiv 4\pi N z_v e \beta / \epsilon$, is just the potential rise coming from the double layer of charge formed by the hexagonal ionic array and its image array when the discrete charges in these arrays are smeared in their planes.² Here N is the number of adsorbed ions per unit area, z_v their valence, β the effective distance shown in Fig. 1 from the imaging plane of the electrode to the charge centroid of an adsorbed ion, and ϵ an effective dielectric constant. The charge density of adsorbed ions is thus $q_1 \equiv N z_v e$, and $N = (4/3r_1^4)^{1/2} \cong 1.1547005 r_1^{-2}$ for a hexagonal array.

The introduction of the dielectric constant ϵ , which we use throughout, has been discussed in I. In the

present case, for adsorption from a gas phase it will be unity if the adions are taken to have negligible induced or permanent dipole moment and if there is nothing between them on the adsorbent. By taking ϵ greater than unity, situations where these conditions do not hold can be treated approximately, although a complete, discrete treatment of all interacting charge multipoles present would be a more accurate approach.² In the electrolyte case, the space in the plane between adsorbed ions is largely or entirely filled with water molecules having both an induced and a permanent dipole moment. The use of $\epsilon > 1$ in the present work is intended to account for the effects of these multipoles (and their images) together with those associated with the polarizability of the adions themselves. When the planar spacing between both induced and permanent discrete dipoles is great enough that they may be well approximated by ideal dipoles, the microscopic, discrete treatment appearing in earlier work² is applicable and leads to an effective ϵ greater than unity as well as other corrections depending upon induced polarization. Here, we make the approximation of subsuming all polarization effects in a dielectric constant ϵ (which should be both space and field dependent—both neglected herein). This artifice seems as far as we can go until a self-consistent, discrete treatment taking proper account of all charges and high multipoles present is worked out. Such a treatment should include thermal-agitation effects; these we also neglect in the present work except to note in passing that, when kT is small compared to the energy of adsorption and lateral interaction, as it usually is, thermal agitation will be small and will simply introduce to first approximation a small temperature- and charge-density-dependent term in the specific adsorption energy. More precise conditions for the validity of the present treatment are discussed below.

As becomes evident later, the present exact treatment of an infinite array of nonpolarizable adsorbed ions with free space between them in the plane leads to solutions for the potential and fields which are made up of closed-form parts plus infinite series contributions. The series parts become negligible as $r_1 \rightarrow 0$, holding z fixed, or as $z \rightarrow \infty$, holding r_1 fixed. In many cases of practical interest, the series contributions are negligible. In the case of z fixed and $r_1/\beta \rightarrow \infty$, the situation approaches a discrete array of ideal dipoles. The series contributions of the present solution then become dominant, making calculation lengthy. Luckily, however, this is just the situation which has been treated in earlier work² (where the effect of induced polarizability of the adions is also included in a self-consistent way), and we thus now have useful and accurate solutions which span the entire range of $0 \leq r_1/\beta < \infty$.

When the image picture is appropriate, the method of images allows the potential outside either a good conductor or a strong dielectric to be determined for certain classes of bounding surfaces, including the plane.

² J. R. Macdonald and C. A. Barlow, Jr., *J. Chem. Phys.* **39**, 412 (1963); **40**, 237 (1964); *J. Phys. Chem.* **68**, 2737-2740 (1964): "Theory of Work-Function Change on Adsorption of Polarizable Ions," *J. Chem. Phys.* (to be published).

The image method employed here requires that β be negligible compared to both the minimum radius of curvature of the adsorbing surface and its minimum lateral dimension. Further, the classical image-force law breaks down if the charge being imaged is too close to the imaging surface. This situation has been investigated quantum mechanically,^{3,4} and it has been found that the classical image-force law leads to a potential contribution only about 9% too large in magnitude for a value of β of 1 Å. Further,⁵ no deviations in emitted current from the Fowler-Nordheim theory of field emission based on the classical image-force potential were observed by Barbour *et al.* until the field exceeded about 5×10^7 V/cm. Since the value of β will not usually be appreciably less than 1 Å and the maximum field in the inner layer of the electrolyte double layer apparently⁶ does not exceed about 3×10^7 V/cm, we use the classical image law in the present work.⁷

In the section on rearrangement and adsorption energy, we define pertinent potentials and examine rearrangement and adsorption energies, quantities which have been incorrectly related in the prior literature. Finally, after a critique of prior work on the micro-potential problem, we discuss in detail results of our exact single-imaging calculations.

GLOSSARY

General Quantities

(x, y, z)	Components of position vector, the positive z axis lying along the outward normal of the electrode
(X, Y, Z)	Normalized position vector $\equiv \beta^{-1}(x, y, z)$
β	Distance from electrode to adsorption plane
γ	Distance from adsorption plane to arbitrary point
r_1	Nearest-neighbor distance in array
R_1	$\beta^{-1}r_1$
ϵ	Effective dielectric constant
z_v	Valence of adions
T	Absolute temperature
N	Surface number density of adions (also, total number of adions)

q_1	Surface charge density on adsorption plane $\equiv z_v e N$
q	Electrode surface charge density
L_1, L_2	Normalized coordinates parallel to adsorption plane
f	$-\psi_2/\psi_\infty \equiv$ proportion of total potential traversed by an ion being adsorbed
f'	$-\psi_{i2}/\psi_\infty \equiv$ quantity analogous to f but including self-image contribution
U	Total system energy
ΔU	Energy change accompanying adsorption \equiv adsorption energy
W	Rearrangement work
U_{int}	Nearest-neighbor interaction energy
W_1	Work necessary to bring charge from OHP to IHP based on calculation of Mott and Watts-Tobin
W_2	Work necessary to bring charge from OHP to electrode based on calculation of Mott and Watts-Tobin
ϵ_{MW}	Electric field according to Mott and Watts-Tobin
ϵ_{dip}	$-2z_v e \sigma \beta / \epsilon r_1^3 \equiv$ field at (0, 0, 0) associated with array of ideal dipoles
ϵ_{Mig}	Field based on a calculation of Mignolet
ψ_{dip}	$2z_v e \sigma \beta^2 / \epsilon r_1^3 \equiv$ potential at (0, 0, 1) associated with ideal-dipole array
σ	11.034175 \equiv a number associated with ideal-dipole hexagonal arrays
η	Value of $N \Delta \psi_a(1) / \psi_a(1)$
τ	$\psi_a(1) / \psi_{a1}(1)$
λ	$\gamma / (\beta + \gamma)$
Λ	ψ_1 / V_{1m}
Δ	$(\Lambda / \lambda) - 1$
Δ_0	Value of Δ when $q=0$
Δ_0^0	Value of Δ when $q=0$ and $\beta=\gamma$
m^{-1}	Maximum value of $d(-q_1)/dq$
γ_1	Euler-Mascheroni constant $\cong 0.57721566$

³ J. Bardeen, Phys. Rev. **49**, 653 (1936).

⁴ P. H. Cutler and J. J. Gibbons, Phys. Rev. **111**, 394 (1958).

⁵ D. Nagy and P. H. Cutler, Phys. Rev. Letters **10**, 263 (1964).

⁶ J. R. Macdonald and C. A. Barlow, Jr., J. Chem. Phys. **36**, 3062 (1962).

⁷ (a) J. O'M. Bockris, M. A. V. Devanathan, and K. Müller, Proc. Roy. Soc. (London) **A274**, 55 (1963). (b) This paper also appears in *Proceedings of First Australian Conference on Electrochemistry*, edited by J. A. Friend and F. Gutmann (Pergamon Press, Ltd., Oxford, England, 1965), pp. 832-863.

An unfortunate but necessary complication has been the requirement of carefully distinguishing between many related but not identical potentials. The notation used has been chosen so as to suggest the definitions which follow.

Local Potentials

ψ_{aic}	Potential arising from complete adion-image array
ψ_e	Potential contribution from excess charge $q+q_1$ on the electrode
ψ_{ic}	$\psi_e + \psi_{aic} \equiv$ complete potential for complete array
ψ_a	Potential analogous to ψ_{aic} but pertaining to a lattice with a single vacancy
ψ	$\psi_a + \psi_e \equiv$ potential analogous to ψ_{ic} but for the single vacancy case
ϕ_{ic}	Potential due to a charge at $(0, 0, 1)$ and its image at $(0, 0, -1)$
ϕ_{iZ}	Potential due to the image of a charge at $(0, 0, Z)$
ϕ_{i1}	ϕ_{iZ} with the image taken to be at $(0, 0, -1)$
ψ_i	A hybrid potential $\equiv \psi + \phi_{iZ}$
ψ_{ai}	$\psi_a + \phi_{iZ} \equiv \psi_i - \psi_e$
ψ_{ai1}	$\psi_a + \phi_{i1} \equiv$ a special case of ψ_{ai}

Potential Differences

ψ_{a1Z}	$\psi_a(1) - \psi_a(Z)$
$\psi_{a1\infty}$	$\psi_a(1) - \psi_a(\infty)$
ψ_{ai1Z}	$\psi_{ai}(1) - \psi_{ai}(Z)$
$\psi_{ai1\infty}$	$\psi_{ai}(1) - \psi_{ai}(\infty)$
ψ_1	$\psi(1) - \psi(Z) \equiv$ the conventional micropotential
ψ_{i1}	$\psi_i(1) - \psi_i(Z) \equiv$ the correct micropotential
ψ_2	$\psi(1) - \psi(\infty)$
ψ_{i2}	$\psi_i(1) - \psi_i(\infty)$

} Near-field micropotentials

Average Potentials and Potential Differences

ψ_∞	$4\pi N_{zv} e\beta / \epsilon \equiv$ average potential for $Z > 1$ arising from adion-image array
V	Average potential including the effect of ψ_e , i.e., the effect of excess charge, $q+q_1$, on the electrode
V_0	Total PD from electrode to bulk of electrolyte
V_1	The PD from electrode to OHP (across inner layer)
V_2	The PD from OHP to bulk of electrolyte (across diffuse layer)—usually ignored
V_{1m}	$\psi_\infty [Z(q/q_1) + (Z-1)]$ an artificial function used for normalization

Fields (Z Components)

\mathcal{E}_{aic}	Field arising from complete adion-image array, associated with ψ_{aic}
\mathcal{E}	Field associated with ψ_a
\mathcal{E}_0	\mathcal{E} evaluated at $(0, 0, 0)$
\mathcal{E}_1	\mathcal{E} evaluated at $(0, 0, 1)$
E_∞	$-\psi_\infty / \beta \equiv$ average value of \mathcal{E} or \mathcal{E}_{aic}

REARRANGEMENT AND ADSORPTION ENERGY

Before considering these energies, it is convenient to introduce some normalized quantities and pertinent

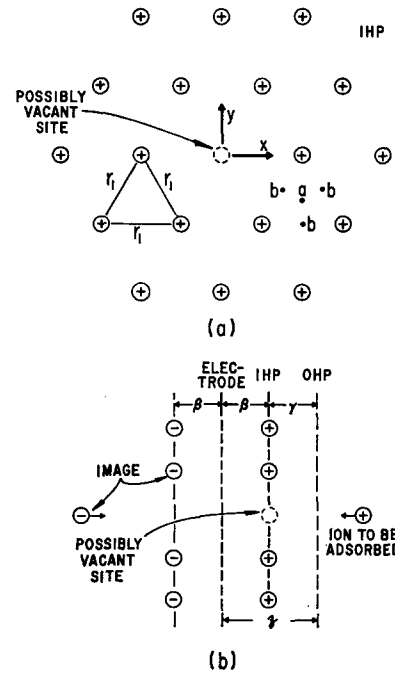


FIG. 1. Hexagonal lattice of adsorbed ions: (a) Plane of adions showing coordinates, nearest-neighbor distance r_1 , and Points a and b ; (b) cross-sectional view showing images and the distances β , γ , and z .

potentials. Referring to Fig. 1, let $r_1/\beta \equiv R_1$, $x/\beta \equiv X$, $y/\beta \equiv Y$, and $z/\beta = (\beta + \gamma)/\beta \equiv Z$. Note that Z , as well as X and Y , is variable since γ may take on all values from $-\infty$ to ∞ . For the electrolyte case, a specific choice of a finite value of γ may be used to define the OHP, as in Fig. 1(b). Let the contribution (calculated later) to the actual potential at some point (X, Y, Z) outside the electrode arising only from the complete array of discrete adions and their images be denoted by $\psi_{aic}(X, Y, Z)$. When X and Y are zero and attention is restricted to the line perpendicular to the electrode through the central adsorbed charge (or vacancy), denote the potential contribution $\psi_{aic}(0, 0, Z)$ by $\psi_{aic}(Z)$, etc.

When the adsorbing plane is grounded, its average charge density q will be just $-q_1$, and there will be no

average field far outside the adsorbed array. This is not so for an arbitrary q , and we must then add the contribution ψ_e to the total potential arising from an externally impressed PD which causes $q \neq -q_1$. Simple electrostatics show that in the present case the average potential outside the electrode $V(X, Y, Z) \equiv V(Z)$ is

$$V(Z) = -\psi_\infty [Z(q/q_1) + (Z-1)u_0(Z-1)], \quad (1)$$

where $u_0(Z)$ is the Heaviside unit step function, zero for $Z < 0$, unity for $Z > 0$. The contribution to the total potential arising from the externally impressed PD is then $\psi_e(X, Y, Z) \equiv \psi_e(Z) = V(Z) - [V(Z)]_{q \rightarrow -q_1}$, or

$$\psi_e(Z) = -\psi_\infty Z [1 + (q/q_1)]. \quad (2)$$

The complete potential for a full array is then,

$$\psi_{ic}(X, Y, Z) \equiv \psi_{aic}(X, Y, Z) + \psi_e(Z). \quad (3)$$

In discussing the micropotential, it is frequently of interest to define two further potentials $\psi_i(Z)$ and $\psi(Z)$. The first of these contains a contribution from the image of a charge at Z but no contribution from the charge itself (at either Z or 1). The latter potential contains no contribution from either the charge or its image and thus applies to an array complete except for a central vacancy. If we define $\psi_a(Z)$ as the direct contribution arising only from the ions and their images of this incomplete array, then

$$\psi(Z) \equiv \psi_a(Z) + \psi_e(Z) \quad (4)$$

is the potential along the line normal to the adsorbent through the vacant site.

At a point (X, Y, Z) the contribution to the potential from an adion charge at $(0, 0, 1)$ and its image at $(0, 0, -1)$ is, in terms of normalized quantities,

$$\phi_{ic}(X, Y, Z) = \left(\frac{z_0 e}{\epsilon \beta R_1} \right) \left\{ \left[\left(\frac{X}{R_1} \right)^2 + \left(\frac{Y}{R_1} \right)^2 + \left(\frac{Z-1}{R_1} \right)^2 \right]^{-\frac{1}{2}} - \left[\left(\frac{X}{R_1} \right)^2 + \left(\frac{Y}{R_1} \right)^2 + \left(\frac{Z+1}{R_1} \right)^2 \right]^{-\frac{1}{2}} \right\}. \quad (5)$$

Then, we have, for example,

$$\psi_{aic}(Z) \equiv \psi_a(Z) + \phi_{ic}(Z). \quad (6)$$

The contribution to the potential from the image of a charge of valence z_v at $(0, 0, Z)$ but including no contribution from the charge itself is

$$\phi_{iz}(Z) = -z_v e / 2\epsilon \beta Z, \quad (7)$$

and we may now form

$$\psi_{ai}(Z) \equiv \psi_a(Z) + \phi_{iz}(Z) \quad (8)$$

and

$$\begin{aligned} \psi_i(Z) &\equiv \psi_{ai}(Z) + \psi_e(Z) \\ &\equiv \psi(Z) + \phi_{iz}(Z). \end{aligned} \quad (9)$$

Later, we require the potential along the line through the vacant site, including the contribution of the image of an adion charge at this site $(0, 0, 1)$ but not including

any contribution from the charge itself. From the foregoing, we can write

$$\psi_{ai}(Z) \equiv \psi_a(Z) + \phi_{ai}(Z), \quad (10)$$

where $\phi_{ai}(z) \equiv -z_v e / \epsilon \beta (Z+1)$. The quantity equivalent to ψ_{ai} in I was there termed $\phi_a(\mathbf{R})$.

Let us reserve the term "micropotential" for the conventional electrolyte micropotential (which applies to a full array minus a single central adion and its image). Let us define further

$$\psi_{a1Z} \equiv \psi_a(1) - \psi_a(Z),$$

$$\psi_{a1\infty} \equiv \psi_a(1) - \psi_a(\infty) = \psi_a(1) - \psi_\infty,$$

$$\psi_{aiZ} \equiv \psi_{ai}(1) - \psi_{ai}(Z),$$

and

$$\psi_{ai1\infty} \equiv \psi_{ai}(1) - \psi_{ai}(\infty) = \psi_{ai}(1) - \psi_\infty.$$

Then the micropotential, $\psi_1 = \psi(1) - \psi(Z)$ is, in the present single-imaging case,

$$\begin{aligned} \psi_1 &= \psi_{a1Z} + \psi_\infty (Z-1) [1 + (q/q_1)] \\ &= \psi_{a1Z} + (4\pi\gamma/\epsilon) (q + q_1). \end{aligned} \quad (11)$$

In this definition of the micropotential, we have omitted the small PD V_2 which occurs across the diffuse part of the electrolyte double layer (taken smeared, not discrete). This term may always be added in where appropriate.^{6,8} Since q_1 never equals $-q$ in the electrolyte case (because of the charge q_2 in the diffuse layer), the second term in (11) will always be important.

In a similar way, we may define $\psi_{i1} \equiv \psi_i(1) - \psi_i(Z)$, the correct micropotential, which includes the image contribution. This becomes

$$\psi_{i1} = \psi_1 - (z_v e / \epsilon) (\gamma / 2\beta^2 Z). \quad (12)$$

Finally, in the case of adsorption onto a grounded electrode from a gas phase, we may further define two near-field micropotentials: $\psi_2 \equiv \psi(1) - \psi(\infty)$ and $\psi_{i2} \equiv \psi_i(1) - \psi_i(\infty)$. For $q = -q$ these become

$$\psi_2 = \psi_{a1\infty}, \quad (13)$$

$$\psi_{i2} = \psi_{ai1\infty}. \quad (14)$$

Note that $-\psi_2/\psi_\infty \equiv f = 1 - [\psi_a(1)/\psi_\infty]$ measures the proportion of the total potential ψ_∞ which an ion traverses in being brought from "infinity" to its position at the vacant site at the IHP. This quantity, or its equivalent, calculated in an approximate fashion, has appeared in a number of treatments⁹⁻¹¹ of ionic

⁸ J. R. Macdonald and C. A. Barlow, Jr., in Ref. 7(b), pp. 119-247.

⁹ N. S. Rasor, C. Warner, III, and A. R. Vernon, *Atomics International Report No. AI-6799* (November 1961). See especially pp. 108-109.

¹⁰ A. J. Kennedy, *Advan. Energy Conversion* **3**, 207 (1963). Reference to other papers where the method is used (primarily for three-dimensional lattices) is given in Ref. 23.

¹¹ J. W. Gadzuk, *MIT Quarterly Progress Report No. 72* (15 January 1964), pp. 166-171. See also J. W. Gadzuk and E. N. Carabateas, *J. Appl. Phys.* **36**, 357 (1965). In the latter paper, the authors claim complete rigor for their calculations of f but actually treat the adsorbed charge and its image as an ideal dipole.

adsorption such as the adsorption of cesium ions on a tungsten surface. More pertinent, however, is

$$f' \equiv -\psi_{iz}/\psi_{\infty} = 1 - [\psi_{ai}(1)/\psi_{\infty}],$$

which includes the image contribution. Note that $f' = f + z_v e / (2\beta e \psi_{\infty})$. Improved calculations of f with polarizable ions are in progress.

From the definition of the true micropotential, it is clear that this potential, $\psi_{ai} \equiv \psi_i(1) - \psi_i(Z)$, which enters into the adsorption isotherm, gives the work needed to bring unit charge from some reference surface ($Z = \text{constant}$), sometimes taken at "infinity", to the adsorption site, given the single vacancy, the array of adions, and the array of images (including the self-image, the image of the removed charge). Note that this does *not* represent the adsorption energy, the actual system energy change associated with adsorption of the additional adion, for two reasons: (1) The self-image adsorption energy includes a factor of $\frac{1}{2}$ which is missing here; (2) The rearrangement energy required to produce the vacancy and make room for the additional ion to be adsorbed does not vanish as stated by Grahame¹² but generally is of the same order of magnitude as the quantity $z_v e \psi_a(1)$, as is shown by Eq. (16).

We may relate $\psi_{ai}(1)$ to the adsorption energy ΔU as follows. Considering the adsorbing surface to be a sphere of arbitrarily large radius and for illustrative purposes specializing to the case $q = -q_i$, we find the total system energy is given by the expression $U = (z_v e / 2) \sum_{\text{adions}} \psi_{ai}$, where ψ_{ai} is evaluated at the adion sites ($Z = 1$ plane); therefore, $U = (z_v e / 2) \psi_{ai}(1) N$ for unit area and given N . The factor $\frac{1}{2}$ enters from two sources: (1) In that part of $\psi_{ai}(1)$ arising from adions directly, the factor $\frac{1}{2}$ must be included to avoid counting adion-pair interaction energies twice; (2) In that part of $\psi_{ai}(1)$ arising from images, $\phi_{i1}(1)$, the factor $\frac{1}{2}$ takes into account the usual reduction of particle-image-pair interaction energy from that occurring in particle-particle interactions. We see then that the Boltzmann factor which is generally used in statistical treatments of adsorption contains for the present case a part, $\exp\{- (1/kT) \sum_{\text{adions}} z_v e \psi_{ai}(1)\}$, which involves *twice* the system energy (referred to an infinite separation of charges), or $2U$. That this is the correct dependence for systems such as we are concerned with is shown elsewhere.¹³

We now enquire for a single additional adion ($\Delta N = 1$), "What is the adsorption energy?" and "What is the rearrangement work?" It is simple to determine these quantities for the present case of adsorption on a large sphere, inasmuch as the edge effects which otherwise would prove bothersome are in this case nonexistent. Clearly, the potential at any point in the vicinity of the adsorption surface is, for the indefinitely large sphere, arbitrarily close to that obtained from an in-

finite planar array. We, therefore, may use the general expression quoted earlier for the total electrical energy of the system, identifying the potentials occurring there with those appropriate to the planar array. One then obtains for the total system energy change including rearrangement,

$$\begin{aligned} \Delta U &= U(N+1) - U(N) \\ &= (z_v e / 2) [\Delta N \psi_{ai}(1) + N \Delta \psi_{ai}(1)] \\ &= (z_v e / 2) [\psi_{ai}(1) + N \Delta \psi_{ai}(1)] \\ &= (z_v e / 2) [\psi_{ai}(1) + N \Delta \psi_a(1)]. \end{aligned} \quad (15)$$

In a limited range of adsorption about N , one may set $\Delta \psi_a(1) / \psi_a(1) \equiv \eta \Delta N / N = \eta / N$, and $\psi_a(1) / \psi_{ai}(1) \equiv \tau$, where η and τ are taken constant in the limited range of N . One obtains $\Delta U = (z_v e / 2) \psi_{ai}(1) (1 + \eta \tau)$, $\psi_{ai}(1) \neq 0$. For the special case $\psi_{ai}(1) = 0$, one finds $\Delta U = (z_v e / 2) \eta \psi_a(1) = - (z_v e / 2) \eta \phi_{i1}(1)$. From the definitions, the rearrangement work is $W \equiv \Delta U - z_v e [\psi_a(1) + (\frac{1}{2}) \phi_{i1}(1)]$. One readily finds

$$\begin{aligned} W &= (z_v e / 2) [\eta \tau \phi_{i1}(1) + (\eta \tau - 1) \psi_a(1)] \\ &= (z_v e / 2) (\eta - 1) \psi_a(1). \end{aligned} \quad (16)$$

Note that for $\psi_{ai} = 0$, Eq. (16) may be written

$$W = (z_v e / 2) (1 - \eta) \phi_{i1}(1). \quad (17)$$

Now it turns out that in the regime $|\psi_a(1)| \gg |\phi_{i1}(1)|$, W is quite negligible; in this case $R_1 \ll 1$ and one readily finds that $\eta \approx 1$ and that $\tau \approx 1$. In the limit, therefore, Grahame's result, $W = 0$, is perfectly correct. In the opposite extreme, $|\psi_a(1)| \ll |\phi_{i1}(1)|$, we have that $R_1 \gg 1$, the adions and their images are closely approximated by ideal dipoles,¹⁴ and $\eta \approx 1.5$. Since for this case τ is negative and $|\tau| \ll 1$, it follows that $W \approx (z_v e / 4) \tau \psi_{ai}(1) \equiv (z_v e / 4) \psi_a(1)$ is indeed of the order quoted above and is much less in magnitude than the full adsorption energy. It is in the intermediate case, $|\psi_a(1)| \sim |\phi_{i1}(1)|$ and hence $R_1 \sim 1$ (within a decade, say), where the departure of W from zero is most important: Here again $\tau \sim 1$, but as may be seen from the exact calculated values displayed in Fig. 2 η typically lies in the range $1.2 < \eta < 1.5$. Thus, here we have $W \sim (z_v e / 6) \psi_a(1)$, a quantity of the same order as the adsorption energy ΔU and hence not at all negligible. This is significant insofar as this range is the one of primary physical importance. Also shown in Fig. 2 for comparison with the η curve is a curve of $1.5 \psi_a(1) / \psi_{dip}$, where ψ_{dip} , the potential at $(0, 0, 1)$ arising from a surrounding infinite hexagonal array of ideal dipoles, is $2z_v e \sigma \beta^2 / e r_1^3 \approx (317.76132 / \epsilon) / (\beta R_1^3)$ V. Here $\sigma \approx 11.034175$ for a hexagonal array and β is in angstroms in the second expression for ψ_{dip} . Note that Fig. 2 indicates that $\psi_a(1) \approx \psi_{dip}$ when R_1 is of the order of 10 or greater.

¹² D. C. Grahame, Z. Elektrochem. **62**, 264 (1958).

¹³ C. A. Barlow, Jr., Am. J. Phys. **31**, 247 (1963).

The flaw in Grahame's "proof"¹² that $W=0$ for the general case is simply that of equating an expression for the energy of a charged spherical capacitor (valid only for spherical equipotential surfaces and continuous charge distributions) with the energy of the actual discrete system of charges. This approach ignores discreteness of charge from the outset, considers a system for which rearrangement is unnecessary for the addition of more charge, and therefore incorrectly leads to the result $W=0$. We remind the reader, however, that although the nonvanishing of the rearrangement work is pertinent to the question of the adsorption energy, it does not bear upon the value of the micropotential quantity appearing in the Boltzmann factor¹³ which determines the amount of adsorption in the conventional formulations. It was pointed out earlier that the micropotential does not include the rearrangement work and certain other quantities which must be included in the full adsorption energy.

DISCUSSION OF EARLIER SINGLE-IMAGE TREATMENTS

We have already mentioned a self-consistent treatment of the single imaging problem in which the non-ideal dipoles of spacing 2β are approximated as ideal dipoles.² Bockris, Devanathan, and Müller⁷ have attempted an improvement on this type of approach (but without the self-consistency feature, since they neglect induced polarizability of adions) by using the first two terms in the binomial expansion of $[\tau^2 + (2\beta)^2]^{-1/2}$ and thus treating slightly nonideal dipoles. A much superior approach suggested earlier^{2,8} is the combination of the self-consistent approach with a better, approximate formula for nonideal dipoles derived by Mignolet.¹⁴ This formula is considered below.

Grahame¹² has calculated a few values of what is essentially $\psi_a(1)$ by directly summing the contributions from a finite number of surrounding adions. His results are too small by 4% to 5%, showing that he ceased

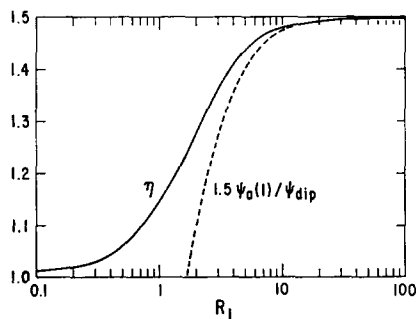


FIG. 2. Dependence of the differential adsorption quantity $\eta = N\Delta\psi_a(1)/\psi_a(1)$ on R_1 and comparison with $1.5\psi_a(1)/\psi_{dip}$.

¹⁴ J. C. P. Mignolet, Bull. Soc. Roy. Sci (Liège) **23**, 422 (1954).

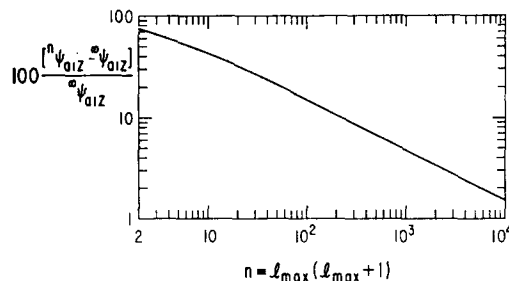


FIG. 3. Percent inaccuracy of the approximate micropotential quantity ${}^n\psi_{aiz} \equiv {}^n\psi_a(1) - {}^n\psi_a(Z)$ vs n , the number of adion-image terms whose contribution was included in the sum yielding ${}^n\psi_{aiz}$. ${}^\infty\psi_{aiz} \equiv \psi_{aiz}$. $r_1 = 5 \text{ \AA}$, $q_1 \cong 74 \mu\text{C}/\text{cm}^2$, $\beta = \gamma = 2 \text{ \AA}$, $\psi_{aiz} \cong -4.83/\epsilon\text{V}$, $R_1 = 2.5$, and $Z = 2$.

summing too soon. The pertinent sum for a hexagonal array may be written using oblique contravariant coordinates as

$$\psi_a(Z) = \frac{6z_0e}{\epsilon\beta} \sum_{l=1}^{\infty} \sum_{m=0}^{l-1} \times \{[(Z-1)^2 + p^2 R_1^2]^{-1/2} - [(Z+1)^2 + p^2 R_1^2]^{-1/2}\}, \quad (18)$$

where

$$p^2 = l^2 + m^2 - lm. \quad (19)$$

Unfortunately, the convergence of this series is very slow, as shown in Fig. 3, unless $R_1/Z \gg 1$. Of course both $\psi_a(Z)$ and $\psi_a(1)$ must be calculated to obtain the micropotential. Figure 3 shows that for the specific case considered, more than 2×10^4 terms in ψ_{aiz} (or more than 8×10^4 individual square-root terms) must be calculated to achieve even 1% accuracy in ψ_{aiz} .

Several authors^{10,15,16} have employed a compromise method in which the first p nearest neighbors are summed and the remainder of the sum replaced by an integral which could be carried out explicitly. Although this method can yield sufficient accuracy for practical purposes provided the break point between summation and integration is chosen wisely, it is rather cumbersome, and the results of the present treatment or these joined to those in Ref. 2 are generally simpler and preferable. It is noteworthy that Gomer¹⁵ actually calculated some values of $\psi_{aic}(X, Y, Z)$ for four different positions [one of them being that marked "a" in Fig. 1(a)] in the XY plane using the summation-integration method.

An entirely different approach has been used by Buff and Stillinger.¹⁷ They treat the case of partial imaging (including infinite and single imaging) and sum up the contributions perpendicular to the electrode arising

¹⁵ R. Gomer, J. Chem. Phys. **21**, 1869 (1953). Gomer has employed the same method to treat imaging of dipoles: L. W. Swanson and R. Gomer, J. Chem. Phys. **39**, 2813 (1963).

¹⁶ I. Langmuir, J. Am. Chem. Soc. **54**, 2798 (1932).

¹⁷ F. P. Buff and F. H. Stillinger, Jr., J. Chem. Phys. **39**, 1911 (1963).

from a given charge and its infinite number of partial images by means of the Fourier-Bessel integral method. Their result, applied to a hexagonal array, must still be summed in the plane (a double summation), and it is the slow convergence of this summation which leads to difficulties in the actual application of any such method. Actually, in the limit of single imaging, their doubly infinite sum of integrals must reduce to a sum such as that of (18).

In fact, Buff and Stillinger, having found the contribution from a single line of images, then proceed to treat a situation entirely different from that where lattice sums are appropriate. In comparing their work with that of the present authors, one must accordingly expect somewhat differing results arising from the contrasting models employed. The essential difference between the two treatments is in the degree of long-range order assumed: Treatments such as the present one are most appropriate when the degree of such order is high, when a lattice structure tends to form over the surface, and when thermal disordering may be considered to be a small effect over distances no larger than that characterizing the effective range of interaction in the plane. The model of Buff and Stillinger is the complete opposite. There, it is implicitly assumed that thermal disordering is so nearly complete that (1) one need only consider low-order interaction-induced correlations in particle position, ignoring higher-order distribution functions; (2) the thermally averaged, or expectation value, potential obtained by integration is the quantity which is appropriate to represent the system. Both of these assumptions naturally fail utterly when a two-dimensional lattice starts to form: The first fails because a lattice displays such extreme regularity that the one- and two-particle distribution functions manifestly do not supply a complete representation of the system; the second assumption loses all its utility inasmuch as the distribution functions reduce to δ functions, requiring that the integrations be replaced by sums over lattice points, as carried out in the present work.

Although Buff and Stillinger argue that imaging in the electrode will so reduce interaction in the plane as to make their treatment most appropriate, an approximate estimate of the six-nearest-neighbor interaction energy, based on a hexagonal array with the ideal-dipole approximation, yields for the reasonable values (see later discussion) $\epsilon=6$ and $\beta=3 \text{ \AA}$, $U_{\text{int}}/kT \sim 125/[R_1^2 r_1(\text{\AA}) kT(\text{eV})] \sim 14$ for $R_1=5$ and room temperature. This result suggests that the array should be a close approximation to a rigid hexagonal structure under these experimentally appropriate conditions. A more precise calculation¹⁸ using accurate potentials calculated by the present method instead of using the ideal-dipole approximation and nearest-neighbor inter-

actions only suggests, however, that for the above parameter values and single imaging $R_1=5$ (corresponding to an area per adion of $\approx 195 \text{ \AA}^2$) is about at the limit of stability for a hexagonal array. The present conditions, together with $R_1=5$, correspond to an adsorbed charge density of $q_1=8.22 \mu\text{C}/\text{cm}^2$. For $|q_1|$ somewhat greater than this value, say at least 10 or 12 $\mu\text{C}/\text{cm}^2$, the fixed-hexagonal-lattice assumption should be an excellent approximation and much more pertinent than the model of Buff and Stillinger. Under these conditions, the "spurious lattice structures" to which they refer need not arise only from ion-size effects as they imply and are evidently not in the least spurious. On the other hand, for $|q_1|$ less than perhaps 5 or 6 $\mu\text{C}/\text{cm}^2$, the Buff-Stillinger model might be applicable. Unfortunately, it appears that for the electrolyte case ($\epsilon \lesssim 5$) there exists a range of adsorption for which the lattice ordering is neither so good nor so negligible as to make either model an excellent description of the situation.

Mott and Watts-Tobin¹⁹ have presented an approximate but readily carried out calculation of the work corresponding to ψ_{01z} for single imaging. Their procedure involves replacing the discrete images in the electrode by a uniform sheet of charge and the discrete adions by a uniform sheet containing a circular vacancy of radius $r_0 = (\pi N)^{-1/2} \approx 0.5250376 r_1$ centered at the origin. Thus, it is only through r_0 that a vestige of discreteness effects remains.

A straightforward calculation in terms of unnormalized variables shows that the electric field at $(0, 0, z)$ \mathcal{E}_{MW} is given in this approximation by

$$\begin{aligned} \mathcal{E}_{\text{MW}} &= -\frac{2\pi N e z_v}{\epsilon} + \frac{N e z_v}{\epsilon} \int_{r_0}^{\infty} \frac{2\pi \gamma r dr}{(\gamma^2 + r^2)^{3/2}} \\ &= -\frac{2\pi N e z_v}{\epsilon} [1 - \gamma(\gamma^2 + r_0^2)^{-1/2}]. \quad (20) \end{aligned}$$

Mott and Watts-Tobin next integrate the field to find the work required to bring a charge from the OHP at $(0, 0, z)$ to the IHP at $(0, 0, \beta)$. The result may be written exactly as

$$W_1 = -(2\pi N e^2 z_v^2 / \epsilon) [\gamma - (\gamma^2 + r_0^2)^{1/2} + r_0]; \quad (21)$$

however, they have taken $\gamma \ll r_0$, which leads to $W_1 \approx -(2\pi N e^2 z_v^2 / \epsilon) \{ \gamma - [\gamma^2 / (2r_0)] \}$, their result except for a typographical error.²⁰

The work W_2 required to bring a charge from $(0, 0, z)$ to the electrode at $(0, 0, 0)$ is, in the present case,

$$W_2 = -(2\pi N e^2 z_v^2 / \epsilon) [\beta + \gamma - (\gamma^2 + r_0^2)^{1/2} + (\beta^2 + r_0^2)^{1/2}]. \quad (22)$$

¹⁸ J. R. Macdonald and C. A. Barlow, Jr., "Thermal Stability of an Adsorbed Array of Charges in the Einstein Approximation," *Can. J. Chem.* (to be published).

¹⁹ N. F. Mott and R. J. Watts-Tobin, *Electrochim. Acta* **4**, 79 (1961).

²⁰ Compilations of typographical and other errors in this and a number of other papers in the present field are given in Ref. 8.

When $(\beta + \gamma) \ll r_0$, (essentially equivalent to $R_1/Z \gg 1$), this becomes

$$W_2 \cong - (2\pi N e^2 z_0^2 / \epsilon) \{ \beta + \gamma - [(\gamma^2 - \beta^2) / (2r_0)] \}. \quad (23)$$

Finally, again for $(\beta + \gamma) \ll r_0$ one may write,

$$W_1 = (2\pi N e^2 z_0^2 / \epsilon) (\gamma^2 / 2r_0) + \lambda_1 W_2, \quad (24)$$

where $\lambda_1 \equiv [\gamma / (\beta + \gamma)] [2r_0 / (2r_0 + \beta - \gamma)]^{-1}$. Now, for $|\beta - \gamma| \ll 2r_0$, $\lambda_1 \cong \lambda \equiv \gamma / (\beta + \gamma)$, the form used by Mott and Watts-Tobin, and the last term in (24) becomes equivalent to Grahame's earlier result,¹² the term involving γ^2 in (24) being the Mott-Watts-Tobin discreteness correction. Although this result is an improvement over those obtained from treatments which entirely neglect discreteness effects, it turns out that, in general, the model is too crude a representation of a discrete system to reliably reproduce even the main features of the behavior of such structure-sensitive quantities as the micropotential, even in the case $\beta \sim \gamma$ and $(\beta + \gamma) \ll r_0$. Finally, it is worth pointing out that although the above treatment was carried out under the implicit assumption $q = -q_1$, Mott and Watts-Tobin finally replaced the above W_2 by the proper $W_2(q)$ in their later analysis. Their ψ , the potential corresponding to $W_2(q)$, is actually equivalent to the present average potential $V(Z)$ of Eq. (1) for $Z \geq 1$. This quantity, in turn is $-V_1$, where V_1 is, in the notation we have used in earlier work, the difference between the average potential at the electrode and that at the OHP.

Grahame¹² originally suggested another approximate method which is a considerable improvement over that put forward later by Mott and Watts-Tobin. In Grahame's "cutoff" method, which has recently been employed by Levine, Bell, and Calvert,²¹ the actual discrete-adion charge distribution is again replaced by a uniform sheet of charge containing a circular vacancy of radius $r_0 = (\pi N)^{-1/2}$ and the image charge distribution is taken smeared but also containing a colinear circular vacancy of radius r_0 . This approximation, as used by Grahame and by Levine *et al.* for single imaging, leads to some β dependence of W_1 , missing in the simpler, Mott-Watts-Tobin calculation.

In spite of the above improvement, we have shown that the cutoff method greatly overestimates the effect of discreteness at the IHP in the infinite-imaging situation,¹ where the effect is actually quite small, at least at $q = 0$, and we show later that this approach, when properly applied, also somewhat overestimates it in the present single-imaging case, where the effect is large.

It is worth pointing out that discreteness-of-charge effects do not disappear at elevated temperatures where a fixed hexagonal array breaks into a disordered, semirandom array. Thus, there is no assurance that the cutoff results are superior to the present ones at high

temperatures where $U_{\text{int}}/kT \gtrsim 1$. Even the approach of Buff and Stillinger, while an improvement for this situation, involves only thermal mean values and does not provide for calculating all discreteness effects in the limit of a disordered but still discrete array. In the single-imaging cutoff approximation case, Levine *et al.* have actually only calculated a quantity ϕ''_{β} equivalent to $\psi_{a\infty}$. Unfortunately, their prescription for forming the micropotential ψ_1 is incorrect in the single-imaging (or partial-imaging) case where $\psi_a(Z) \neq 0$. In the infinite-imaging case with which Levine *et al.* were primarily concerned, $\psi_a(Z) = 0$ and the general expression used for ψ_1 was correct. To calculate ψ_1 properly for single imaging on the cutoff model, we require the quantity $\psi(Z)$, not given by Levine *et al.* or Grahame. A simple calculation leads to

$$[\psi(Z)]_{\text{cutoff}} = [\psi_a(Z)]_{\text{cutoff}} + \psi_e(Z),$$

where $\psi_e(Z)$ is given in Eq. (2) and

$$[\psi_a(Z)]_{\text{cutoff}} = (\psi_{a\infty} / 2) \times \{ [(\tau_0/\beta)^2 + (Z+1)^2]^{1/2} - [(\tau_0/\beta)^2 + (Z-1)^2]^{1/2} \}. \quad (25)$$

From this result, we can calculate needed quantities for comparison with the present accurate hexagonal array solution. Such comparison is carried out later.

SERIES TRANSFORMATIONS

In order to calculate $\psi_{aic}(X, Y, Z)$ and/or $\psi_a(Z)$ accurately without excessive use of digital-computer time, it is desirable to express these quantities in terms of series which converge far more rapidly than does, for example, that of Eq. (18) for $\psi_a(Z)$. We have investigated a number of approaches to this problem. First, Fig. 3 shows that direct summation of (18) even with a digital computer is impractical if R_1 values of the order of and less than 5 are of interest. One method we used primarily for checking results was to consider the equivalent screened Coulomb-potential problem in which $\psi_a(Z, \theta)$ is written, for a hexagonal array, in exactly the same form as (18) but with the exponential cutoff term $\exp(-\theta p)$ multiplying each of the terms in the series. One then calculates values of $\psi_a(Z, \theta)$ for several values of θ , such as 0.2, 0.1, 0.05, and extrapolates the results, using the epsilon algorithm²² for example, to $\theta = 0$ to yield $\psi_a(Z)$. Although this procedure does shorten total computing time, this still remains quite long and the value obtained for $\psi_a(Z)$ is not very accurate when R_1 is small.

Alternatively, to obtain $\psi_a(1)$, we may use our rapidly convergent infinite-imaging series with progressively larger values of γ (or Z), then extrapolate the results to $\gamma = \infty$. Finally, we tried transforming the infinite-imaging series analytically to obtain a rapidly convergent single-imaging series. Unfortunately, we did not obtain such a series independent of the arbitrary

²¹ S. Levine, G. M. Bell, and D. Calvert, *Can. J. Chem.* **40**, 518 (1962).

²² P. Wynn, *Chiffres* **4**, 23 (1961); J. R. Macdonald, *J. Appl. Phys.* **35**, 3034 (1964).

parameter s appearing in this approach. Thus, it was again necessary to calculate values with several values of s and extrapolate to the $s = \infty$ value. These approaches were both somewhat more economical than the above exponential cutoff method, but both required rapidly increasing computer time as R_1 decreased. This is inherent in the Ewald type of transformation used in the infinite-imaging approach and would have occurred even if extrapolation to $s = \infty$ had been unnecessary. In the final method we used, which gives results in agreement with those of all the above methods, the final transformation series are of a quite different kind and converge more and more rapidly as $R_1 \rightarrow 0$.

The final method we applied to the present problem has been described for other series by van der Hoff and Benson,²³ who attribute it to Mackenzie.²⁴ It involves the use of Jacobi's imaginary transformation for theta functions and is applied to the present problem in Appendixes I and II. The result given there for either $\psi_{aic}(X, Y, Z)$ or $\psi_a(Z)$ consists of a closed form part and a series part, with the contribution from the latter becoming negligible when $R_1 \rightarrow 0$ (Z fixed) or $Z \rightarrow \infty$, r_1 fixed. In our actual calculations, all potentials and fields were calculated with a digital computer although the series contributions could frequently be neglected. In the succeeding sections, the results of calculations using the formulas of Appendixes I and II are discussed in detail.

MICROPOTENTIAL RESULTS

In this section, we deal with an incomplete array and thus are primarily concerned with the electrolyte micropotential problem. Some of the potential results also apply, however, to adsorption from a gas phase of an ion on a conducting surface. Further, some comparison between incomplete array and complete array potentials and fields are presented in the next section.

There has been little agreement on the values of β and γ most appropriate in the usual electrolyte situation. Values suggested for β have ranged from²⁵ 0.69 to^{21,26} 3 Å and those for γ from²⁶ 1 to¹ 7 Å. For KI, which we discussed in I and again use as an illustration here, β is not likely to be much less than 2 Å on anodic polarization since this is approximately the radius of the I^- ion. Even should such an adion be somewhat flattened by the high pressures present in the inner layer, some contribution to β must be included arising from field penetration into the outer-surface region of the (mercury) electrode. For many ions, one might

guess that $1.5 \text{ \AA} \leq \beta \leq 3 \text{ \AA}$. The value $\gamma = 7 \text{ \AA}$ discussed in I was a maximum expected magnitude when the adion remains hydrated on the side away from the electrode. A minimum value in this case might be 5 Å. Should the adion not remain hydrated in this direction, γ might be as small as 2 or 3 Å, although it is difficult to see how it could be quite as small as 1 Å. Further, when $\gamma/(\beta + \gamma) \gtrsim 0.6$ and is independent of q_1 , Grahame's²⁷ data for KI together with Eq. (1) for $V(Z)$ show that $V_1 \equiv -V(Z)$ may go through zero and change sign as V_0 , the total potential from the electrode to the bulk of the electrolyte, increases positively. It does not appear, however, that the condition $V_1 = 0$ would necessarily show up strongly in experimental

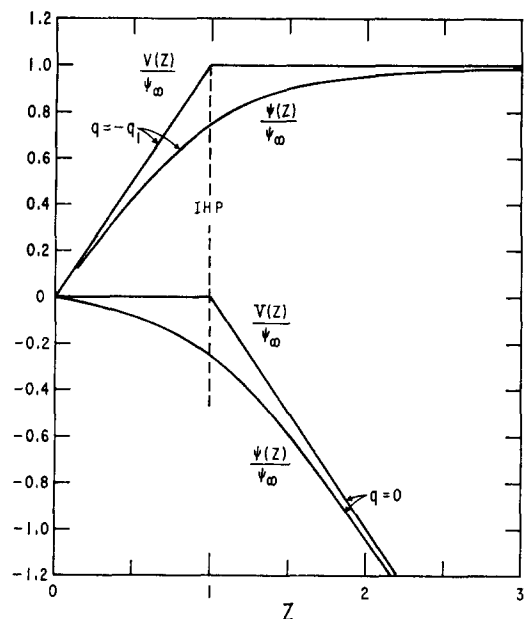


FIG. 4. Dependence of normalized average and accurate ("discrete model") potentials on normalized position Z for $R_1 = 1$ and $q = -q_1$, $q = 0$. If $\beta = 2 \text{ \AA}$, then $r_1 = 2 \text{ \AA}$, $q_1 \cong 462.5 \text{ \mu C/cm}^2$, and $\psi_\infty \cong 104.5/\epsilon V$.

electrolyte data. Specific possible values of β and γ are discussed further at the end of this section. Note that if adions are spherical (and the ionic charge may be taken localized at the center) and remain so on adsorption, the smallest physically realizable value of R_1 is 2, corresponding to close packing on the surface.

Figures 4–6 show how the average potential $V(Z)$ and the accurate potential $\psi(Z)$, both normalized to their common value at "infinity" ψ_∞ , vary with Z for various R_1 values and two different q_1 conditions. As one might expect, Figs. 4 and 5 show that $\psi(Z)$ roughly follows $V(Z)$ but is a smoothed version of it. Further, as shown in Fig. 5(b), as R_1 becomes greater than about 5, $\psi(Z)$ approaches quite closely a linear distance

²³ B. M. E. van der Hoff and G. C. Benson, *Can. J. Phys.* **31**, 1087 (1953).

²⁴ J. K. Mackenzie, thesis, University of Bristol, Bristol, England, (1950).

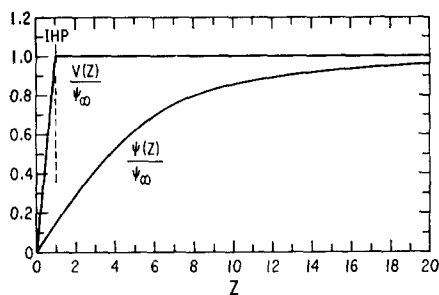
²⁵ R. J. Watts-Tobin, *Phil. Mag.* **6**, 133 (1961).

²⁶ J. M. Parry and R. Parsons, *Trans. Faraday Soc.* **59**, 241 (1963).

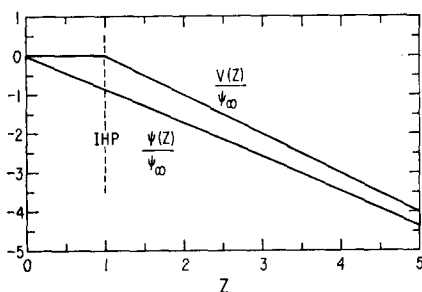
²⁷ D. C. Grahame, *J. Am. Chem. Soc.* **80**, 4201 (1958).

dependence for the $q=0$ case. The curve shown for $R_1=10$ is almost, but not quite, a straight line.

Figures 7 and 8 show comparisons between accurate hexagonal array results and those of the approximate cutoff model. Note that $f \equiv 0$ when the adion array is smeared and discreteness-of-charge effects are ignored. It is surprising how relatively closely the cutoff curves follow the hexagonal array ones. Since $f_{\text{outoff}} < f_{\text{hex}}$, $|\psi_a(1)_{\text{outoff}}| > |\psi_a(1)_{\text{hex}}|$, and the dotted curve of Fig. 7 shows the percent by which the cutoff model, as employed by Levine *et al.*,²¹ overestimates the hexagonal $|\psi_a(1)|$. In the important experimental



(a)



(b)

FIG. 5. Dependence of normalized average and accurate potentials on normalized position Z for $R_1=10$ and for (a) $q=-q_1$, and (b) $q=0$. If $\beta=2 \text{ \AA}$, then $r_1=20 \text{ \AA}$, $q_1 \cong 4.625 \text{ \mu C/cm}^2$, and $\psi_{\infty} \cong 1.045/\epsilon \text{ V}$.

range for electrolytes of $2 < R_1 \leq 10$, we see that the cutoff model is actually quite inaccurate. Note that it could be modified to yield results much closer to those of the hexagonal array, however, by using say $r_0 \cong 0.63 r_1$ rather than the relation quoted earlier.

To the degree that the unmodified cutoff model yields results in agreement with the approach of Buff and Stillinger,¹⁷ the cutoff predictions may be superior to those of the hexagonal array at sufficiently large R_1 's that thermal disordering has effectively destroyed the hexagonal arrangement. When this is the case, however, the adion charge concentration will frequently be too small to affect experimental results very much.

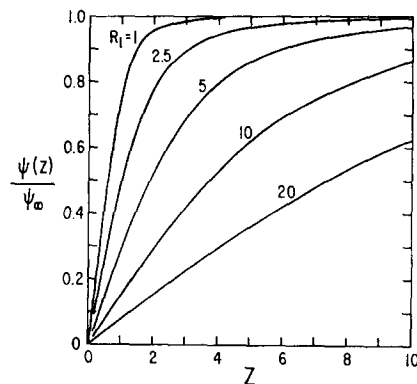


FIG. 6. Dependence of $\psi(Z)/\psi_{\infty}$ on Z with $q=-q_1$ for a variety for R_1 values.

As Fig. 8 shows, comparison involving the discreteness-of-charge part of the micropotential ψ_{a1Z} is somewhat more complicated than that involving $\psi_a(1)$ alone. Below a certain R_1 which depends on Z , the cutoff model underestimates the magnitude of the array value, while it overestimates it by 20% to 25% when R_1 is appreciably greater than the crossover value. Again, the cutoff model could be made to yield results closer to the hexagonal array values by using $r_0 \cong 0.63 r_1$ and also by increasing $|\psi_{a1Z}|_{\text{outoff}}$ values by about 5%.

It turns out experimentally that for values of Z likely in the electrolyte situation, such as $2 \lesssim Z \lesssim 4$, the quantity $[\psi_e(1) - \psi_e(Z)]$ will be of greater magnitude than, and of opposite sign to, ψ_{a1Z} for all pairs of values of q and q_1 associated by an adsorption isotherm, where $(q+q_1)$ has the same sign as z_v . Thus, when $|\psi_{a1Z}|$ is overestimated, for example, by the cutoff model compared to the hexagonal-array result, then the micropotential $|\psi_1|$ will correspondingly be underestimated.

Since several writers on the electrolyte micropotential have suggested that

$$\psi_1 \cong [\gamma/(\beta+\gamma)]V_1 \equiv \lambda V_1 \quad (26)$$

to good approximation even in the single imaging case, it is of interest to investigate this approximation for

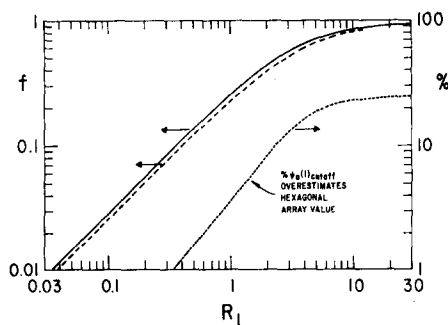


FIG. 7. Dependence of $f \equiv 1 - [\psi_a(1)/\psi_{\infty}]$ on R_1 and percentage overestimate of accurate hexagonal results by the cutoff model. — Hexagonal array; - - - cutoff model.

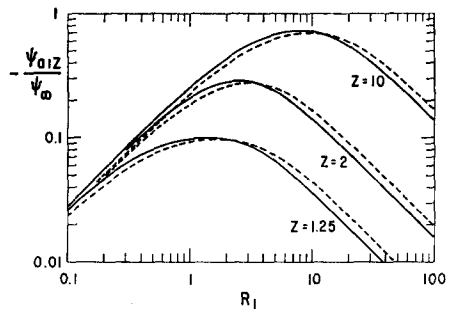


FIG. 8. Comparison of hexagonal array and cutoff model results for the micropotential quantity $\psi_{01z} \equiv \psi_0(1) - \psi_0(Z)$ for several Z values. — Hexagonal array; --- cutoff model.

the present single-imaging case. Let us therefore define

$$\Lambda \equiv \psi_1/V_{1m} \equiv \lambda[1 + \Delta], \quad (27)$$

where

$$V_{1m} = \psi_\infty [Z(q/q_1) + (Z-1)]. \quad (28)$$

Here $V_{1m} = -V(Z) \equiv V_1$ for $Z \geq 1$; it is the natural continuation of $-V(Z)$ with no discontinuity in $dV(Z)/dZ$ at $Z=1$ for $Z \leq 1$. We normalize with V_{1m} rather than V_1 for completeness so that Λ may be defined and plotted for $Z < 1$ [where $V(Z)$ may be zero] as well as $Z > 1$.

Figures 9 and 10 show how Λ varies with R_1 for various values of Z when $q=0$ and $-q_1$. Note that for $q=0$, all curves approach that of f , already discussed, when R_1 is sufficiently large. Since $\psi_e(Z) \equiv 0$ and $V_{1m} \equiv -\psi_\infty$ when $q = -q_1$, the upper curves of Fig. 10 are, for equivalent Z , identical except for different

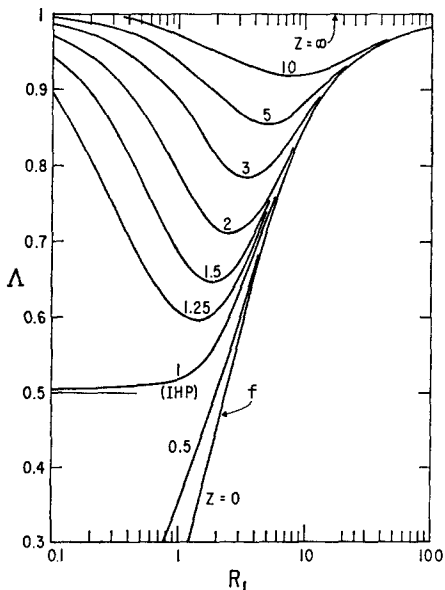


FIG. 9. The quantity $\Lambda \equiv \psi_1/V_{1m}$ vs R_1 for $q=0$ and several values of Z showing (for $Z \geq 1$) how the micropotential differs from the macropotential. The limiting curve marked f is identical with the solid curve of Fig. 7 but is shown here with a linear ordinate scale.

ordinate scales to the solid curves of Fig. 8. The curves shown for $Z < 1$ are related to the difference in potential or energy necessary to bring a test charge from a position $(0, 0, Z)$ in the incomplete hexagonal array to the IHP at $Z=1$. Like the normalized curves for $Z > 1$, they depend strongly on the values of q and q_1 .

The quantity Δ of Eq. (27) shows how much ψ_1 differs from a simple linear dependence on V_{1m} or V_1 . Let us further define, as in I, Δ_0 as the value of Δ when $q=0$ and Δ_0^0 as the value when $q=0$ and $\beta=\gamma$. Then Fig. 11 gives a comparison of several predictions of Δ_0^0 vs R_1 . We see that the discreteness correction of Mott and Watts-Tobin to linear dependence on V_1 is very poor for almost all R_1 values. In agreement with the results of Fig. 8, the cutoff model, on the other hand, follows the hexagonal-array results reasonably well. Note, however, that the values of Δ_0^0 are quite large

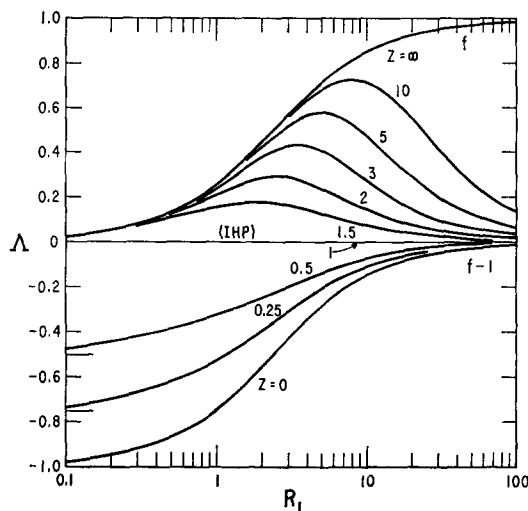


FIG. 10. The quantity Λ vs R_1 for $q = -q_1$ and several Z values. Note the limiting curves of f and $(f-1)$.

and are nowhere near negligible. The largest values of the hexagonal Δ_0^0 in the experimental range of R_1 was about 0.05 for infinite imaging¹; here the smallest value is about 0.5!

We have already mentioned the semi-ideal-dipole single-imaging treatment of Bockris, Devanathan, and Müller.⁷ Its results are not shown in Fig. 11 for the following reasons. First, in this calculation of the micropotential, the contribution from the externally impressed PD, $\psi_e(Z)$, is not taken into account properly. Thus, the separation between average-charge and discrete-charge effects is much worse than even that of the treatment of Mott and Watts-Tobin. In fact, this deficiency leads (when plausible values are used of four undefined quantities in the Bockris *et al.* treatment) to Δ_0^0 values which are always more negative than -0.3 for all values of R_1 . The same difficulties, of course, apply as well to Δ values for which $q \neq 0$. Even were the average discrete separation

made correctly in a treatment of the type discussed, its results would be only slightly better than those of the usual ideal-dipole approach and would be considerably worse than those following from the cutoff model.

Figure 12 shows how the hexagonal array Δ_0 varies with R_1 for various Z values. For Z near 1, Δ_0 does not depend much on R_1 , and ψ_1 and V_1 are almost proportional, but the proportionality constant is far different from the λ of Eq. (26). Even for $Z=5$, larger than experimentally likely in the electrolyte case, Δ_0 is still too large to neglect and Eq. (26) is still a rather poor approximation. Note that the curves of Fig. 12 approach β/γ as $R_1 \rightarrow 0$ or as $R_1 \rightarrow \infty$. In these limits the proportionality constant is thus unity rather than λ .

For comparison with similar infinite-imaging curves in I, we show in Figs. 13 and 14 how Δ varies with q_1 for two different values of γ . Here q_1 and q both vary and are connected by an adsorption isotherm. The $q_1(q)$ data used were derived by Grahame²⁷ from differential

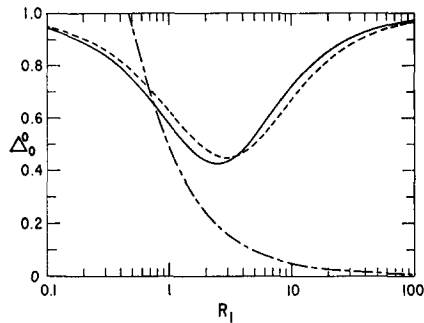


FIG. 11. Normalized discreteness contribution Δ_0^0 vs R_1 for $q=0$, $\beta=\gamma$, $Z=2$, showing deviations of approximate treatments from hexagonal-array results. — Hexagonal array; --- cutoff model; - - - Mott and Watts-Tobin.

capacitance measurements on 1.0*N* KI. As in I, the $\gamma=1$ Δ curve again shows a pole because V_1 can pass through zero for this small a value of γ . Although Δ_0 curves of Figs. 13 and 14 differ greatly from the corresponding infinite-imaging ones, the Δ results are quite similar but with single-imaging curves lying appreciably above the infinite-imaging ones. Thus, the largest value of Δ for $\gamma=7$ Å was about 0.37 for infinite imaging; here it is about 0.46. These values are still much too large to neglect.

It should be emphasized that when V_1 changes sign, a possibility independent of whether infinite or single-imaging models are considered, Δ becomes infinite and the approximation of a linear dependence of ψ_1 on V_1 becomes meaningless. Further, the very large factors (12 for $q_1 = -10$; 2.4 for $q_1 \simeq -40$), by which the cutoff Δ_0^0 results for infinite imaging were found to exceed the hexagonal results, apply for all values of q , not just the $q=0$ value for which comparison is actually made in I; thus, for infinite imaging the cutoff model will yield a much larger deviation from linearity over the

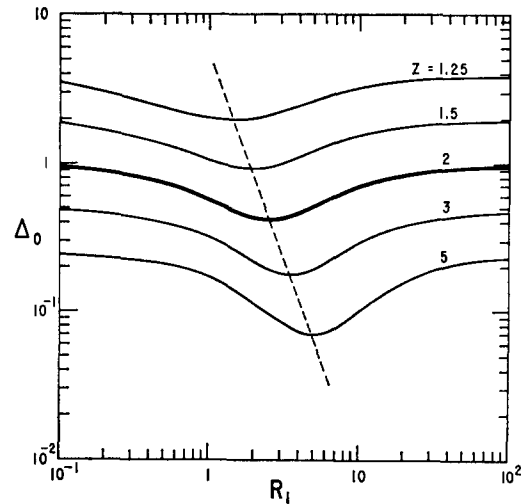


FIG. 12. Normalized discreteness contribution Δ_0 vs R_1 for $q=0$ and several values of Z .

entire $q_1(q)$ range than will the hexagonal, even in regions far from a possible pole.

It should be mentioned that results have been presented both for infinite imaging and single imaging in terms of the quantity Δ , since it is this quantity which measures the validity of the uniform-field approximation, $\psi_1 = \lambda V_1$, already discussed at some length: The condition required for the exactness of the approximation is the vanishing of Δ , which has been shown generally to be more closely the case for infinite imaging than for single imaging. Another quantity which might have been used to describe the micro-potential is the ratio $\Gamma \equiv \psi_1 / [V(1) - V(Z)] \equiv 1 - \delta$, where δ measures the difference between the micro-potential and the macropotential. Space prohibits detailed presentation of curves for these quantities, but the behavior is as anticipated, δ approaching zero for sufficiently small $|q_1/q|$.

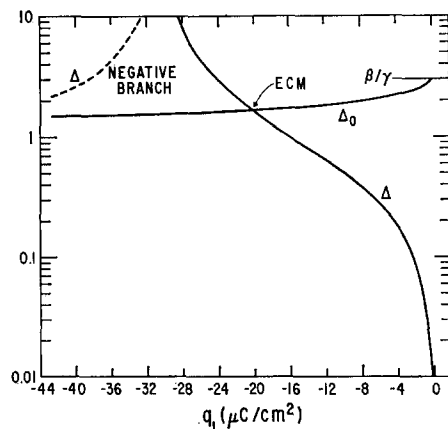


FIG. 13. Normalized discreteness contribution Δ vs Grahame's derived $q_1(q)$ for $\beta=3$ Å, $\gamma=1$ Å, and $Z=\frac{1}{2}$. 1.0*N* KI data.

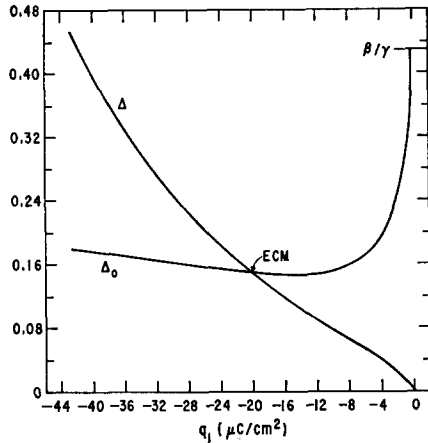


FIG. 14. Normalized discreteness contribution Δ vs Grahame's derived $q_1(q)$ for $\beta=3 \text{ \AA}$, $\gamma=7 \text{ \AA}$, and $Z=10/3$. 1.0N KI data.

Finally, Fig. 15 shows how the three potentials $V(Z)$, $\psi(Z)$, and $\psi_i(Z)$ vary with position for three pairs of q and q_1 values taken from Grahame's 1.0N KI results. We have used $\epsilon=1$ here for convenience in plotting potentials; it should be between about 5 and 15 and should vary with q because of dielectric saturation and compression effects.^{2,8,9}

In Fig. 15(a) for very small adsorption, $\psi(Z)$ is very close indeed to linear and $V(Z)$ is almost but not quite linear, as shown by its dashed extrapolation. The curves of $\psi_i(Z)$, which include the image contribution to the potential, are of particular interest. Since we are here concerned with anion adsorption and $z_v=-1$, the minima in the $\psi_i(Z)$ curves are not positions of stable equilibrium but are instead unstable equilibrium positions. The actual stable position of the adion-charge centroids is taken to be at the IHP. In Figs. 15(a) and 15(b), the field (including image contribution, and calculated with $\epsilon=1$) at the IHP, -8.291×10^7 and -6.606×10^7 V/cm, respectively, tends to urge anions away from the IHP, and the equilibrium must therefore involve steric and "chemical" adsorption forces whose resultant attraction overshadows the repelling electrical force on an adsorbed anion. On the other hand for Fig. 15(c), the maximum observed adsorption, the field at the IHP is only 4.639×10^6 V/cm, and the stable position of equilibrium must be determined almost entirely by the balance between repelling steric forces and attractive "chemical" forces. In the present case, the attractive image-force field alone at the IHP is about $-8z_v \times 10^7$ V/cm. Thus, with $q=18$ and $q_1=-42.61 \mu\text{C}/\text{cm}^2$, the field on a positive rather than negative charge at the IHP will be -1.553×10^8 V/cm and strongly attractive. These fields will all be quite different with partial or infinite imaging, especially if $\gamma \approx \beta$. In spite of the probably relatively poor applicability of the single-imaging model in the electrolyte situation, it is interesting to note the appearance of correct qualitative behavior, namely that as the elec-

trostatic repelling force on the adions increases, the adsorption drops markedly.

An approximate maximum possible value of γ/β may be inferred from the adsorption isotherm and experimental adsorption results. Over most of the experimental range, where the isotherm is well approximated by that of Henry which involves a single Boltzmann factor, we may write

$$\frac{d\psi_{i1}}{d[\ln(q_1/q_{10})]} \approx \left(\frac{kT}{e}\right) > 0, \quad (29)$$

where q_{10} is some constant reference value of q_1 . Since it is found experimentally that $dq_1/dq \leq 0$, the inequality of (29) may be rewritten as

$$\frac{d\psi_{i1}}{d[\ln(q/q_0)]} > 0, \quad (30)$$

where q_0 is a reference value of q . From Eqs. (1), (12),

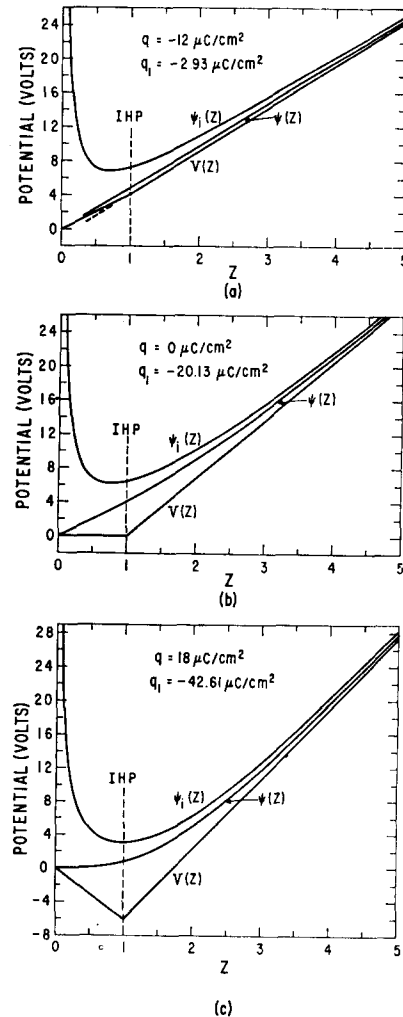


FIG. 15. Variation of several potentials with Z for $\epsilon=1$, $\beta=3 \text{ \AA}$ and three different sets of $q_1(q)$ values associated with Grahame's 1.0N KI results. (a) $R_1 \approx 8.376$ and $\psi_\infty \approx -0.9928$ V; (b) $R_1 \approx 3.195$ and $\psi_\infty \approx -6.821$ V; (c) $R_1 \approx 2.196$ and $\psi_\infty \approx -14.438$ V.

(27), and (30), we may derive the condition

$$(1+\Delta)\left(1+\lambda\frac{dq_1}{dq}\right)+\left(1+\lambda\frac{q_1}{q}\right)\frac{d\Delta}{d[\ln(q/q_0)]}>0, \quad (31)$$

which holds for both infinite and single imaging. Any small dependence of β and γ on q and q_1 has been neglected.

Now let us define $[d(-q_1)/dq]_{\max} \equiv m^{-1}$. For Grahame's 1.5N KI data, $m \sim 2/3$, and if the second term on the left of (31) were negligible as well as $|\Delta|$ compared to unity, we should have $\lambda_{\max} < m \sim 2/3$, leading to $\gamma_{\max} \lesssim 2\beta$. This is the condition which applies when Δ is negligible and ψ_{i1} is proportional to V_1 . Even in the infinite-imaging case, where Δ_0 is quite small, the results of I show that Δ is very appreciable over most of the q_1 range and cannot be neglected.

We illustrate the effect of an appreciable Δ for the present single-imaging case, merely noting that it will be somewhat smaller (allowing a somewhat larger value of γ for given β) in the infinite-imaging case. Rather than calculate all the terms of (31) for single imaging to determine allowable γ 's, we have calculated, using Grahame's 1.0N KI data, a number of curves of ψ_{i1} vs $\ln(q_1/q_{10})$ for a variety of β and γ values. The condition (29) may be directly compared with the slopes of such curves. Figure 16 shows some such curves for $\beta = 2.5 \text{ \AA}$. The dashed curves show the corresponding V_1 results. Since these potentials have actually been calculated with $\epsilon = 1$, we must replace the kT/e in (29) by $\epsilon(kT/e)$ for comparison with the calculated curves. The dot-dash line in Fig. 16 is thus drawn with a slope of $\epsilon(kT/e)$ using a constant $\epsilon = 15$ and $T = 25^\circ\text{C}$, the temperature of Grahame's 1.0N KI experiment which led to the $q_1(q)$ values used in calculating the theoretical curves.

If dielectric saturation varied in the range of $|q_1|$ shown, ϵ would vary, and the dot-dash curve should not be a straight line. (Further, it should drop below the straight line somewhat in the highest adsorption region because of failure of the Henry isotherm.) Actually, we find that with single-image adsorption the field at various points in the inner layer remains large in magnitude and quite constant as q_1 changes. Thus, for $\beta = 3 \text{ \AA}$ and $\gamma = 2 \text{ \AA}$, the field with $\epsilon = 1$ (not including an image contribution) at the point $(0, 0, \frac{2}{3})$ varies only over a range from -1.72×10^8 to $-1.60 \times 10^8 \text{ V/cm}$ for the q range from -14 to 18 \mu C/cm^2 which results in $-q_1$ varying from about 1 to 40 \mu C/cm^2 . It is thus likely that the effective ϵ which should enter the calculation of fields and potentials should be that for an almost completely saturated condition and should perhaps vary no more than from 6 to 8 over the entire q range. A value of 7 still leads to a field magnitude at $(0, 0, \frac{2}{3})$ of over $2 \times 10^7 \text{ V/cm}$, sufficient to yield virtually complete dielectric saturation of surrounding water molecules.⁶

The remarkable constancy of the field arises from the combination of q and q_1 contributions to it. When

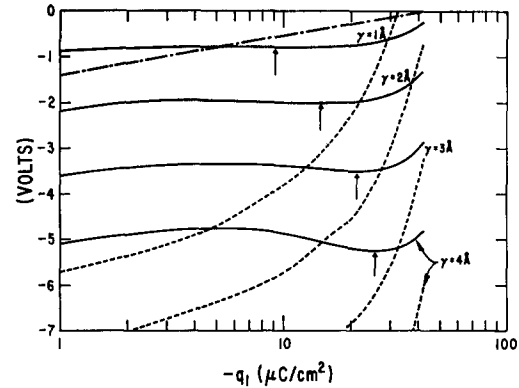


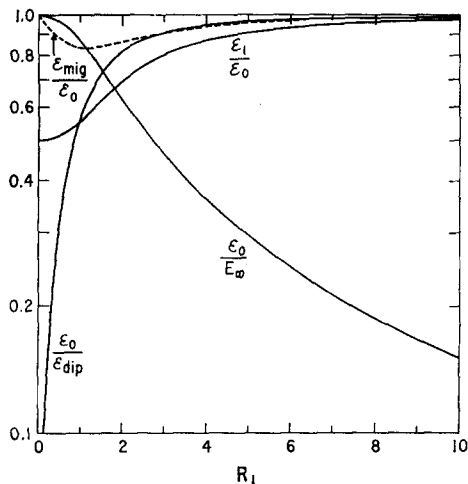
FIG. 16. Variation of the potential differences ψ_{i1} and V_1 with q_1 (log scale) using Grahame's 1.0N KI $q_1(q)$ results for $\epsilon = 1$, $\beta = 2.5 \text{ \AA}$, 25°C , and several values of γ . — ψ_{i1} ; --- V_1 ; ···· see text.

$q \ll -1$, adsorption is negligible and the field $4\pi q/\epsilon$ is dominant. By the time $q=0$, adsorption is quite large for 1.0N KI, and the field arising from the discrete adions is of the same sign and order of magnitude as that with little or no adsorption. Even for $q \gg 1$, the combination of the field associated with $\psi_e(Z)$ and that associated with $\psi_a(Z)$ remains surprisingly constant.

The arrows on the solid curves of Fig. 16 indicate approximate q_1 values where the slope goes through zero and the inequality (29) fails. We note that it fails even for $\gamma = 1 \text{ \AA}$ and that the actual slope at small $|q_1|$, which is again on the right sign, is too small in magnitude unless the effective ϵ should be as small as about 3. Conditions are obviously worse for larger values of γ . For $\beta = 2.5 \text{ \AA}$, the condition $dV_1/dq > 0$, somewhat more applicable for infinite imaging, fails at about $\gamma = 5$, in agreement with earlier conclusions for this case.

We have investigated β values of 2 and 3 \AA as well as the 2.5 \AA shown in Fig. 16. As expected, the inequality (29) fails even worse for $\beta = 2$ than for 2.5 \AA . For $\beta = 3 \text{ \AA}$, however, it does not fail until $\gamma > 2 \text{ \AA}$. The slopes of the $\gamma = 1 \text{ \AA}$ and $\gamma = 2 \text{ \AA}$ curves for $-q_1 \lesssim 10 \text{ \mu C/cm}^2$ are consistent with ϵ values of approximately 7 and 5, respectively. For $\beta = 3 \text{ \AA}$, the condition $dV_1/dq > 0$ just fails for $\gamma = 6 \text{ \AA}$. The slopes of all λV_1 curves for which $dV_1/dq > 0$ are too large over much of the q_1 range, for reasonable ϵ , to allow a potential directly proportional to V_1 to be used in the adsorption isotherm. It is thus fortunate that Δ is not everywhere negligible even for infinite imaging. Notice that for very small $|q_1|$ where the hexagonal model itself is not likely to be a good approximation to the actual state of affairs, Δ is essentially negligible, inapplicability of the model is immaterial, and the slopes of possible ψ_{i1} curves are very close to those of corresponding λV_1 curves.

The above results still allow us to retain either infinite or single-imaging models to explain KI adsorption data provided γ/β is suitably restricted. Since $\beta \simeq 3 \text{ \AA}$ is about the largest reasonable value for KI, it

FIG. 17. Dependence of various field ratios on R_1 .

appears that $\gamma \approx 2 \text{ \AA}$ is near the largest possible value for single imaging and $\gamma \approx 3 \text{ \AA}$ is near the largest value for infinite imaging. These results depend on β and γ remaining independent of $|q_1|$. The small dependence likely because of high-field compression effects is made even smaller by the near constancy of the actual field as q_1 varies. The above values of γ seem to indicate that hydration of anions in the direction away from the electrode is impossible if single, infinite, or partial imaging is an applicable model. It is most unlikely that the effective dielectric constant of a water molecule bound between two ions can be anything but saturated. Thus, such hydration seems to require a γ value of at least 5 \AA , too large for the above models. These questions will be examined quantitatively for partial imaging in the next paper in this series.

Finally, for the incomplete lattice, the dependence of the fields at $(0, 0, 0)$ and $(0, 0, 1)$ on R_1 is of interest. In Fig. 17, we show curves of various field ratios for the case of $q = -q_1$, which eliminates any Z -independent field since ψ_e is then zero. Let us denote the field associated with $\psi_a(X, Y, Z)$ by $\mathcal{E}(X, Y, Z)$ and set $\mathcal{E}(0, 0, 0) \equiv \mathcal{E}_0$ and $\mathcal{E}(0, 0, 1) \equiv \mathcal{E}_1$ for simplicity. Figure 17 shows, as expected, that $\mathcal{E}_1/\mathcal{E}_0 \rightarrow 0.5$ as $R_1 \rightarrow 0$ and approaches unity as $R_1 \rightarrow \infty$. The figure also compares the accurate \mathcal{E}_0 with the smeared value $E_\infty \equiv -\psi_\infty/\beta$ and with the field $\mathcal{E}_{\text{dip}} \equiv -2z_0 e \sigma \beta / \epsilon r_1^3$ at $(0, 0, 0)$ appropriate for an array of ideal dipoles. Clearly, R_1 must be very small for \mathcal{E}_0 to approach E_∞ closely, but R_1 need be no bigger than 3 or 4 for \mathcal{E}_0 to be quite close to \mathcal{E}_{dip} .

Mignolet²⁸ has given a heuristic formula for the interaction energy of an infinite array of nonideal dipoles at the site of a removed dipole (or removed charge and image). By dividing this result by $z_0 e \beta$, one obtains a lower-limit approximation to \mathcal{E}_0 . Mignolet's expression then leads to

$$\mathcal{E}_{\text{Mig}} = 2\mathcal{E}_{\text{dip}} \xi \{ 2[1 + \tan(\frac{1}{2} \tan^{-1} \xi)]^{-1} - 1 \}, \quad (32)$$

²⁸ A. D. Wheelon, J. Appl. Phys. **25**, 113 (1954).

where $\xi \equiv \rho r_1 / 2\beta$. For a hexagonal lattice, Mignolet's approach leads to $\rho = 2\pi(\frac{2}{3})^{1/2} / \sigma \approx 0.65752056$. The dashed curve of $\mathcal{E}_{\text{Mig}}/\mathcal{E}_0$ shows how superior this formula with the above value of ρ is to that for \mathcal{E}_{dip} . If one is concerned only with the range of physical interest, $R_1 \lesssim 1$, then a larger value of ρ is advantageous. The value 0.8685 leads to $\mathcal{E}_{\text{Mig}}/\mathcal{E}_0 = 1$ at $R_1 = 1$ and to somewhat larger values of $\mathcal{E}_{\text{Mig}}/\mathcal{E}_0$ for $R_1 < 1$. For $R_1 > 1$, however, the minimum value of $\mathcal{E}_{\text{Mig}}/\mathcal{E}_0$, which is about 0.965, occurs near $R_1 = 2$, and the ratio thereafter rapidly becomes even closer to unity. Note, however, that an even superior formula for \mathcal{E}_0 [or $\mathcal{E}(0, 0, Z)$] may be derived from the cutoff model and Eq. (25) provided r_0 is taken as about $0.63 r_1$.

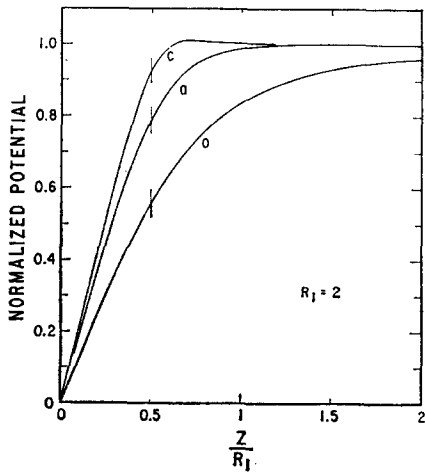
FULL-ARRAY RESULTS

In this section, we are concerned with field and potential variations for a complete hexagonal array with no missing charges. In both work-function and high-field-emission studies, where electrons may emerge from a surface partially covered with adsorbed ions, one is interested in the field and potential at various positions from the adsorbent surface outwards and in the variation of field and potential with adion nearest-neighbor distance. As before, we consider a hexagonal array of adions which are perfectly imaged in the conducting adsorbent plane. In this section, we discuss only the case of a grounded electrode and thus invariably take $q = -q_1$, making $\psi_{ic}(X, Y, Z) = \psi_{aic}(X, Y, Z)$. Further, for convenience, we always take $z_0 = +1$.

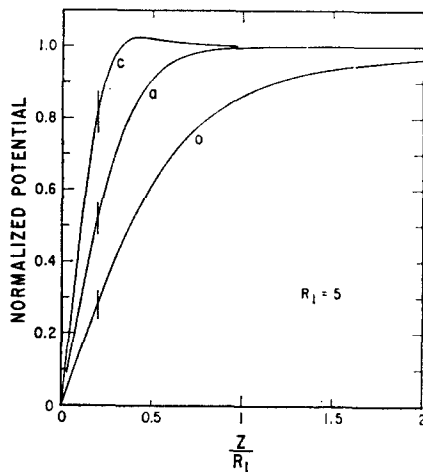
Figure 18 shows, for three different R_1 values, how the potential, normalized with ψ_∞ , varies with distance from the electrode along three different perpendicular lines. One line passes through Point a , shown in Figs. 1 and 21(a). The curves marked c pertain to the perpendicular line which passes through Point c , defined on Fig. 21(b). Point c is one-third of the way along the line bisecting an angle of the basic equilateral triangle of the hexagonal array, just as Point a is two-thirds of the way away from the adion at a vertex of the triangle. Finally, the curves marked o apply in the incomplete array case and are included for comparison. Point o is a point at a triangle vertex, but with the adion and its image belonging there, and only this adion-image pair, removed from the array. Thus, the perpendicular line through o is the line along which it is assumed adsorption occurs and for which the micropotential is defined, as in the last section.

Note that we have used the distance variable $Z/R_1 \equiv (\beta + \gamma)/r_1$ instead of Z in Fig. 18. Such normalization removes, as shown, much of the dependence of curve shape on R_1 which would otherwise appear. Thus, for the complete array, ψ_{aic}/ψ_∞ has always virtually reached unity by $(\beta + \gamma) \lesssim r_1$. Note, however, that the o curves, for ψ_a/ψ_∞ , invariably show considerably slower saturation. Such behavior arises, of course, because the nearest charges are considerably further away from the line through o than they are from the a and c lines. Thus, one must be farther away from the surface along

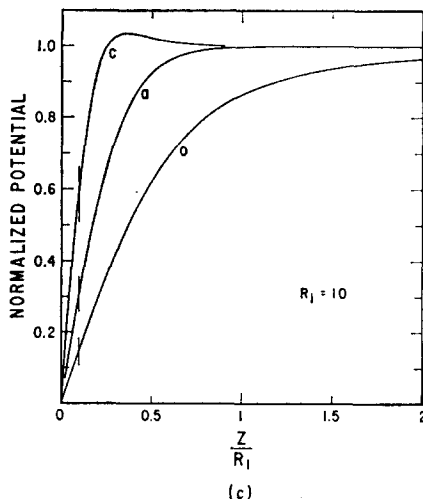
the o line before the smearing approximation is good. For $Z=1$, the charges nearest Point o are R_1 away; for Point a they are $R_1/\sqrt{3}$ away, and for Point c the nearest charge is only $R_1/2\sqrt{3}$ away. The closeness of



(a)



(b)



(c)

FIG. 18. Variation of ψ_{aic}/ψ_{∞} with Z/R_1 for three R_1 values and three lines perpendicular to the adsorbent plane.

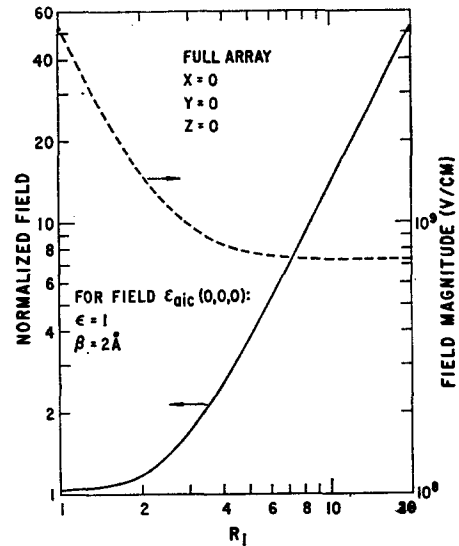


FIG. 19. Dependence of $|\epsilon_{aic}(0, 0, 0)|$ and $\epsilon_{aic}(0, 0, 0)/E_{\infty}$ on R_1 .

Point c to a charge explains why the c curves in Fig. 18 actually overshoot the $\psi_{aic}/\psi_{\infty}=1$ final value slightly. The vertical marks on each of the curves show the positions on the curves where $Z=1$, the plane of the adions themselves. Notice that all of the potential curves are nearly linear between $Z=0$ and $Z=1$. Finally, note that in terms of the present normalization all curve shapes have almost stabilized by $R_1=5$ and there is little further change for larger R_1 .

The field at $X=Y=Z=0$, at the electrode surface immediately between an adion and its image, is shown in Fig. 19. The solid curve is the field normalized with E_{∞} ; the dashed curve is the magnitude of the actual field itself for $\epsilon=1$ and $\beta=2 \text{ \AA}$. For this case, we see that when $r_1 \lesssim 8 \text{ \AA}$ the contributions to the field from neighboring charges and their images have become negligible and, for $z_v=1$, the field is essentially $-2z_v e/\epsilon\beta^2 = -7.1995 \times 10^8/\epsilon \text{ V/cm}$, arising only from the positive charge at $(0, 0, 1)$ and its image in the electrode.

Figure 20 shows the variation with R_1 of normalized potential at points in the plane of adsorbed charge centers. The curve marked b is that for Point b shown in Figs. 1 and 22(b). It is somewhat surprising how close the curves for Points a and b are. In the plane of the charge, the very appreciable difference between the behavior of the potential at Points a and o shows up again just as it did in Fig. 18.

Figure 21 is included to show how the normalized potential at Points a and c depends on R_1 for several different Z values. The solid curves are accurate results calculated by the present approach. The dotted curves included for a few Z values were calculated by Gomer¹⁵ using the summation-integration method mentioned earlier. There seems to be no reason why this method cannot yield reasonably accurate results if sufficient discrete-charge contributions are summed

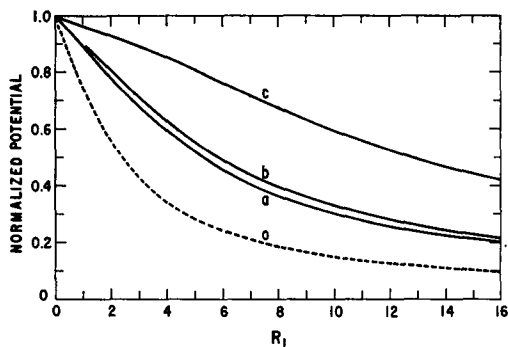


FIG. 20 Comparison of normalized potential dependence on R_1 at $Z=1$ for various points in the plane at the IHP.

before integration is applied. Gomer extended his summations to distances of $4r_1$ from a central charge. This should be sufficient to yield results appreciably more accurate than those shown. Perhaps the discrepancies illustrate the dangers implicit in lengthy and tedious hand calculations. Notice in Fig. 21(b) for Point *c* that again there is a very slight rise of the curves for $Z \geq 2$ over unity and that the maximum of the $Z=0.5$ curve appreciably exceeds the 0.5 limiting value for $R_1=0$.

Since the present analysis allows the field and potential to be calculated anywhere outside the electrode, unlike the more usual crystalline field calculations which yield these quantities only at a lattice point, it is finally of interest to investigate field and potential

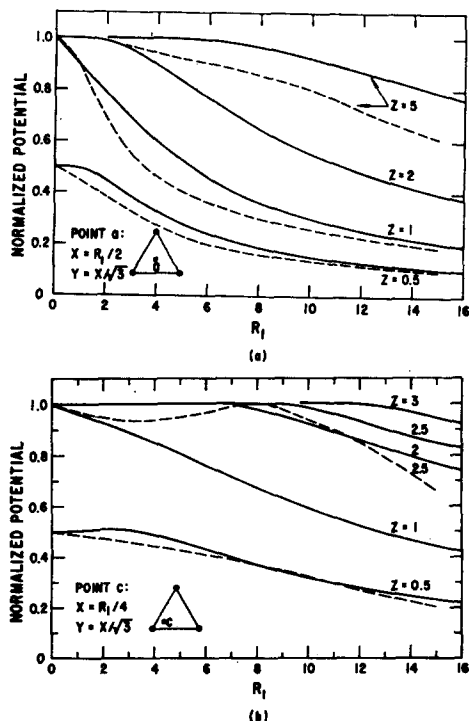


FIG. 21. Comparison of present results (—) and those of Gomer (---) for dependence of normalized potential on R_1 for several Z values. (a) Points on the line passing through Point *a* perpendicular to the adsorbent plane; (b) points on the line passing through Point *c* perpendicular to the adsorbent plane.

variation with position in planes parallel to the adsorbent surface. Figures 22 and 23 show such results. Since the potential is identically zero in the plane of the electrode ($Z=0$), we have shown field dependence (semilog

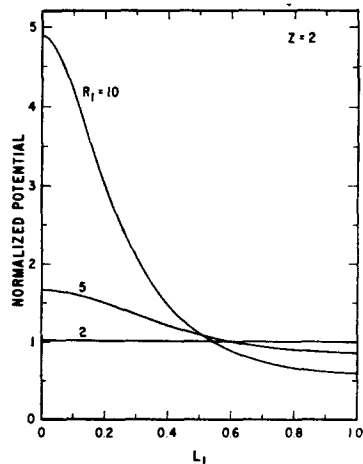
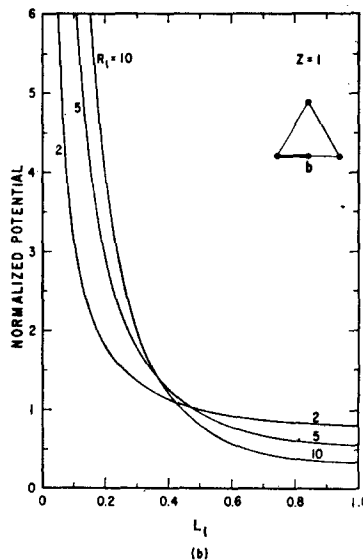
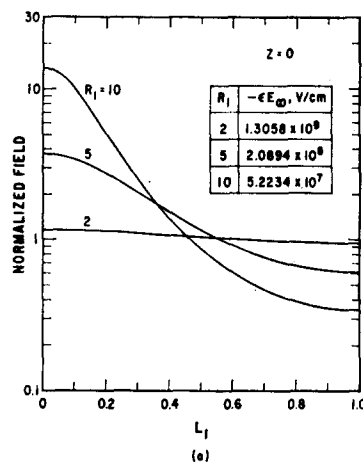


FIG. 22. Variation of normalized field and potential for various R_1 and Z values along the heavy line in the plane shown on the triangle of (b). $L_1 \equiv 2X/R_1$.

ordinate scale) for this plane, and potential dependence (linear scales) for the $Z=1$ and $Z=2$ planes. The field at the surface of the electrode and its variation in the electrode plane is the field of most interest in the

present context anyway, since it is this field which allows determination of potential in the vicinity of the electrode, the quantity most important in affecting such processes as thermionic, photoelectric, and high-field emission.

Figure 22 shows for three R_1 and three Z values the variation of field and potential along the heavy base line of the triangle of Fig. 22(b). For such variation, $Y=0$ and $0 \leq X \leq R_1/2$. The normalized length L_1 is just $2X/R_1$ and is unity when the perpendicular line passing through Point b is reached. Because of the symmetry of the situation, it is unnecessary to show variation in the range $R_1/2 < X \leq R_1$. The present curves all reach their minimum values at the $L_1=1$ point. As expected, for $Z=0$ and $Z=2$ the range of variation of the curves decreases as R_1 decreases until by $R_1=2$ the array is so dense that the field or potential varies very little along the L_1 line. For $Z=1$, however, both field magnitude and potential must go toward infinity as $L_1 \rightarrow 0$, since $(0, 0, 1)$ defines the position of an adion charge. As usual, the charges of adions are approximated in the present calculations as point charges. Since they are actually somewhat distributed for real ions, the potential curves shown for $Z=1$ may be expected to differ somewhat from the real situation for positions sufficiently close to $(0, 0, 1)$.

The table in Fig. 22(a) shows the value of ϵE_∞ for the three R_1 values considered. When the E_∞ normalization is removed from the three field curves of Fig. 22(a), it is found that the values of the field at $L_1=0$ are nearly the same for $R_1=5$ and 10, in agreement with the discussion of Fig. 19.

Figure 23 is like Fig. 22 except that the variation of position is along the angle bisector, the heavy line in the triangle of Fig. 22(b). Here the normalized position variable is $L_2 \equiv 4X/3R_1$, and $Y = X/\sqrt{3}$, $0 \leq X \leq 3R_1/4$. The point of mirror symmetry is at $L_2=1$ but the potential and field curves all reach shallow minima at Point a , shown in the triangle and also on the abscissa scale. Notice that the points at $L_1=0, L_2=0$ are the same, as are those at $L_1=1, L_2=1$. Comparison of corresponding curves of Figs. 22 and 23, taking account of the difference in normalization, show that though they differ in detail the differences are not very large. This is not unexpected since the endpoints of the curves are the same. The table in Fig. 23(c) shows for $\beta = 2 \text{ \AA}$ values of $\epsilon \psi_\infty$ and $\epsilon \psi_{aic}(0, 0, 2)$ which apply for both the L_1 and L_2 curves. The value of $\epsilon \psi_{aic}(0, 0, 2)$ given for $R_1 = \infty$ is just that arising from a single positive charge [at $(0, 0, 1)$] and its image. Thus, the other potential values show the approach to this limiting value as R_1 increases and the contribution from neighboring charges diminishes.

We conclude by discussing how the foregoing results might be applied to thermionic-, field-, or photo-emission from metals covered by an array of adsorbed ions. The first problem in a theory for such effects is to assume a reasonable function for the electric potential in the absence of adsorption and then, in order to

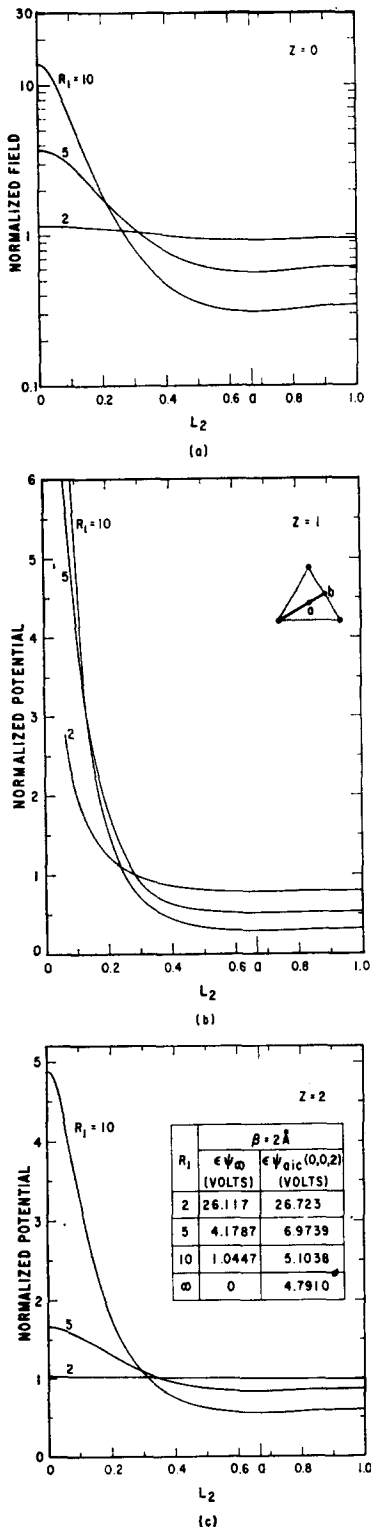


FIG. 23. Variation of normalized field and potential for various R_1 and Z values along the heavy line in the plane shown on the triangle of (b). $L_2 = 4X/3R_1$.

determine the effect of adsorption, to obtain the potential contribution of the adsorbed array. The case of the potential for zero adsorption does not concern us further here; it might be taken to be a step function, let us say.

The interesting question to which the present work relates is the determination of the adion array potential. The method detailed in the Appendixes can be applied to this question and the potential obtained at any desired point; however, it is probably sufficient to approximate the potential by rational functions, for example, so determined that the field at $Z=0$ and the potentials and fields at $Z=1$ and $Z=2$ agree with the results of foregoing sections. The second and, it seems, more difficult question is to find a proper way of using the potential to predict the current density of such processes as thermionic, photoelectric, and high-field emission under adsorption conditions. The main difficulty is that for most situations the de Broglie wavelength of emitted electrons is so long compared with the lateral distance over which the potential varies appreciably that classical physics becomes inapplicable. The solution to the problem of electron emission (but not, for example, proton emission) accordingly requires solution of the Schrödinger equation which describes penetration of the region about the adsorption plane in which the potential varies appreciably. Without actually solving this equation, we are unable to say anything about the effective work-function change (derived from the measured current) other than that it is clearly different from the simple surface-averaged contact potential (obtained, for example, from vibrating capacitor measurements) sometimes used. We believe that this is a quantum-mechanical problem which deserves further attention.

ACKNOWLEDGMENT

The authors gratefully acknowledge the valuable assistance of Charles Ratliff, who wrote the several computer programs required in this work.

APPENDIX I. MAIN RESULTS

Consider a complete planar hexagonal array of charges and the corresponding image array as in Fig. 1. If \mathbf{r} is the vector from the origin at $(0, 0, 0)$ to a given real charge and \mathbf{R} is the vector from $(0, 0, 0)$ to (X, Y, Z) , then

$$\psi_{aic}(\mathbf{R}) = \sum_{\mathbf{r}} (z_v e / \epsilon) [|\mathbf{R} - \mathbf{r}|^{-1} - | \mathbf{R} - (\mathbf{r} - 2\mathbf{i}\beta) |^{-1}]$$

$$= \frac{z_v e}{\epsilon \beta} \left\{ \sum_{l=-\infty}^{\infty} \sum_{m=-\infty}^{\infty} [(S_0^- - S_0^+) + (S_1^- - S_1^+)] \right\}, \quad (A1)$$

where

$$S_{r,\pm} \equiv \left[\left(\frac{X}{R_1} - l - \frac{r}{2} \right)^2 + \left(\frac{Y}{R_1} - \alpha m - \frac{\alpha r}{2} \right)^2 + \left(\frac{Z \pm 1}{R_1} \right)^2 \right]^{-\frac{1}{2}}, \quad (A2)$$

and here $\alpha \equiv \sqrt{3}$, \mathbf{i} is the unit vector in the $+Z$ direction perpendicular to the adsorbing plane, and we have used rectangular coordinates in arriving at the second form of (A1). Now, on using

$$x^{-n} = [\Gamma(n)]^{-1} \int_0^{\infty} t^{n-1} e^{-xt} dt \quad (A3)$$

and defining $P_{r,\pm} = [S_{r,\pm}]^{-2}$, we may write

$$\psi_{aic}(\mathbf{R}) = [z_v e / \epsilon \beta R_1 \Gamma(\frac{1}{2})]$$

$$\times \sum_{l=-\infty}^{\infty} \sum_{m=-\infty}^{\infty} \left(\int_0^{\infty} \{ [\exp(-P_0^- t) - \exp(-P_0^+ t)] + [\exp(-P_1^- t) - \exp(-P_1^+ t)] \} t^{-\frac{1}{2}} dt \right). \quad (A4)$$

This result is next transformed by means of

$$\sum_{l=-\infty}^{\infty} \exp[-(l+a)^2 t] = (\pi/t)^{\frac{1}{2}} \sum_{s=-\infty}^{\infty} \cos(2\pi a s) \exp(-s^2 \pi^2 / t) \quad (A5)$$

to yield

$$\psi_{aic}(\mathbf{R}) = \psi_{aic}(X, Y, Z) = (z_v e / \epsilon \beta R_1)$$

$$\times \sum_{m=-\infty}^{\infty} \sum_{s=-\infty}^{\infty} \left(\int_0^{\infty} \{ [\exp(-V_0^-) - \exp(-V_0^+)] + (-1)^s (\exp(-V_1^-) - \exp(-V_1^+)) \} t^{-\frac{1}{2}} \cos(2\pi s X / R_1) dt \right), \quad (A6)$$

where

$$V_{r,\pm} \equiv \left\{ \left[\left(\frac{Y}{R_1} - \alpha m - \frac{\alpha r}{2} \right)^2 + \left(\frac{Z \pm 1}{R_1} \right)^2 \right] t - \frac{\pi^2 s^2}{t} \right\}. \quad (A7)$$

Finally, we use the relation

$$\int_0^\infty t^{n-1} \exp[-k^2 t - (s^2 \pi^2 / t)] dt = 2(\pi |s| / k)^n K_n(2\pi k |s|), \tag{A8}$$

where K_n is the modified Bessel function of the second kind, to obtain

$$\begin{aligned} \psi_{aic}(X, Y, Z) &= \frac{4z_v e}{\epsilon \beta R_1} \left(\sum_{m=-\infty}^\infty \sum_{s=1}^\infty \cos \frac{2\pi s X}{R_1} \{ [K_0(T_{m0}^-) - K_0(T_{m0}^+)] + (-1)^s [K_0(T_{m1}^-) - K_0(T_{m1}^+)] \} + \frac{1}{2} \sum_{m=-\infty}^\infty \ln \left[\frac{T_{m0}^+ T_{m1}^+}{T_{m0}^- T_{m1}^-} \right] \right); \end{aligned} \tag{A9}$$

the logarithmic terms have appeared from taking the limit of K_0 terms at $s=0$. In this expression $T_{mr^\pm} \equiv T_{mr^\pm}(Y, Z)$, where

$$T_{mr^\pm}(Y, Z) \equiv 2\pi s \{ [\alpha(m + \frac{1}{2}r) - (Y/R_1)]^2 + [(Z \pm 1)/R_1]^2 \}^{\frac{1}{2}}. \tag{A10}$$

The result of Eq. (A9) can be further simplified by using the summation formula Eq. (A25) derived in Appendix III. After simplification, the final result for ψ_{aic} is

$$\begin{aligned} \psi_{aic}(X, Y, Z) &= \frac{z_v e}{\epsilon \beta R_1} \ln \left[\frac{\cosh[4\pi(Z+1)/\alpha R_1] - \cos(4\pi Y/\alpha R_1)}{\cosh[4\pi(Z-1)/\alpha R_1] - \cos(4\pi Y/\alpha R_1)} \right] \\ &+ \frac{4z_v e}{\epsilon \beta R_1} \sum_{m=-\infty}^\infty \sum_{s=1}^\infty \cos \frac{2\pi s X}{R_1} \{ [K_0(T_{m0}^-) - K_0(T_{m0}^+)] + (-1)^s [K_0(T_{m1}^-) - K_0(T_{m1}^+)] \}, \end{aligned} \tag{A11}$$

an expression which applies only for $Z \neq 1$ when $Y=0$. The special case $Z=1$ is treated in Appendix II. Since $K_0(x)$ decreases very rapidly for $x > 1$, all the series terms quickly become small as s increases provided $(Z \pm 1)/R_1 \lesssim 1$. This condition is necessary to ensure rapid convergence of the terms with T_{00}^\pm arguments. We have numerically checked the 6-mm (sixfold) symmetry of (A11).

By differentiation of (A11), one may obtain the electric field in any direction at a given point (X, Y, Z) . Here, we are only concerned with the field in the $+Z$ direction given by

$$\mathcal{E}_{aic}(\mathbf{R}) = \mathcal{E}_{aic}(X, Y, Z) = -(\beta R_1)^{-1} [\partial \psi_{aic} / \partial (Z/R_1)].$$

After differentiation and simplification, we obtain

$$\begin{aligned} \mathcal{E}_{aic}(X, Y, Z) &= \frac{8\pi z_v e}{\epsilon \alpha \beta^2 R_1^2} \frac{\sinh \frac{4\pi}{\alpha R_1}}{\alpha R_1} \\ &\times \frac{\cosh(4\pi Z/\alpha R_1) \cos(4\pi Y/\alpha R_1) - \cosh(4\pi/\alpha R_1)}{\{ \cosh[4\pi(Z+1)/\alpha R_1] - \cos(4\pi Y/\alpha R_1) \} \{ \cosh[4\pi(Z-1)/\alpha R_1] - \cos(4\pi Y/\alpha R_1) \}} \\ &+ \frac{16\pi^2 z_v e}{\epsilon \beta^2 R_1^2} \sum_{m=-\infty}^\infty \sum_{s=1}^\infty s^2 \cos \frac{2\pi s X}{R_1} \{ [(Z-1)/R_1] [(T_{m0}^-)^{-1} K_1(T_{m0}^-) + (-1)^s (T_{m1}^-)^{-1} K_1(T_{m1}^-)] \\ &- [(Z+1)/R_1] [(T_{m0}^+)^{-1} K_1(T_{m0}^+) + (-1)^s (T_{m1}^+)^{-1} K_1(T_{m1}^+)] \}, \end{aligned} \tag{A12}$$

also an equation that does not hold at $Z=1$ when $Y=0$.

The foregoing results apply to a complete array and its image. They may be readily reduced to yield micro-potential quantities by taking $X=Y=0$ and using, e.g., Eq. (6). We find for $Z \neq 1$

$$\psi_a(Z) = (2z_v e / \epsilon \beta R_1) [M(Z) + N(Z)], \tag{A13}$$

where

$$M(Z) \equiv \ln \left\{ \frac{\sinh[2\pi(Z+1)/\alpha R_1]}{\sinh[2\pi(Z-1)/\alpha R_1]} \right\} + \frac{R_1}{Z^2 - 1} [Zu_0(1-Z) - u_0(Z-1)], \tag{A14}$$

and

$$N(Z) = 4 \sum_{m=1}^{\infty} \sum_{s=1}^{\infty} \{ [K_0(T_{m0}^-) - K_0(T_{m0}^+)] + (-1)^s [K_0(T_{m1}^-) - K_0(T_{m1}^+)] \} \\ + 2 \sum_{s=1}^{\infty} \{ [K_0(T_{00}^-) - K_0(T_{00}^+)] + 2(-1)^s [K_0(T_{01}^-) - K_0(T_{01}^+)] \}; \quad (A15)$$

note that $Y=0$ in the T_{mr}^{\pm} arguments. The corresponding field is

$$\mathcal{E}_a(Z) = \frac{z_v e}{\epsilon \beta^2 R_1^2} \left(\frac{(4\pi/\alpha) \sinh(4\pi/\alpha R_1)}{\sinh[2\pi(Z+1)/\alpha R_1] \sinh[2\pi(Z-1)/\alpha R_1]} + \left[\left(\frac{R_1}{Z+1} \right)^2 - \left(\frac{R_1}{Z-1} \right)^2 \operatorname{sgn}(Z-1) \right] \right. \\ + (32\pi^2) \sum_{m=1}^{\infty} \sum_{s=1}^{\infty} s^2 \left\{ \frac{Z-1}{R_1} [(T_{m0}^-)^{-1} K_1(T_{m0}^-) + (-1)^s (T_{m1}^-)^{-1} K_1(T_{m1}^-)] \right. \\ \left. - \frac{Z+1}{R_1} [(T_{m0}^+)^{-1} K_1(T_{m0}^+) + (-1)^s (T_{m1}^+)^{-1} K_1(T_{m1}^+)] \right\} \\ + (16\pi^2) \sum_{s=1}^{\infty} s^2 \left\{ \frac{Z-1}{R_1} [(T_{00}^-)^{-1} K_1(T_{00}^-) + 2(-1)^s (T_{01}^-)^{-1} K_1(T_{01}^-)] \right. \\ \left. - \frac{Z+1}{R_1} [(T_{00}^+)^{-1} K_1(T_{00}^+) + 2(-1)^s (T_{01}^+)^{-1} K_1(T_{01}^+)] \right\} \left. \right). \quad (A16)$$

It has already been mentioned that some of the foregoing results must be modified when $Z=1$; this is done in Appendix II. There are a few other conditions which can lead to trouble with the full hexagonal array equations when $Z=1$. Thus, for example, potentials and fields at the position $(0, \sqrt{3}R_1/2, 1)$ [Point “b” of Fig. 1(a)] cannot be calculated directly with the preceding results. Points with Y near but slightly less than $\sqrt{3}R_1/2$ will also tend to yield inaccurate results. The first of these difficulties may be avoided by carrying out the necessary limits analytically; both may be circumvented by using the symmetry of the full hexagonal array and calculating the desired quantities with the present formulas using different but equivalent points. Thus, for the above representation of Point “b” one could substitute $(3R_1/4, \sqrt{3}R_1/4, 1)$.

APPENDIX II. RESULTS FOR $Z=1, Y=0$

The condition $Z=1$, which restricts attention to the IHP, requires that special limits be carried out to obtain useful expressions for fields and potentials when $Y=0$. Although it is possible to derive such expressions when $X>0$, they are not really needed in the complete array case because the symmetry of the hexagonal array is such that all points with $Z=1, Y=0$, and $X>0$ are equivalent to points with the same X value and $Y=\sqrt{3}X$, loci whose fields and potentials may be calculated using the results of Appendix I, even when $Z=1$. We actually derive results here for $\psi_a(1)$ and for $\mathcal{E}_{aic}(X, 0, 1)$; the expression for the latter will hold for $X=0$ as well and may be readily transformed to yield the field $\mathcal{E}_a(1)$ pertinent to the incomplete micro-potential array.

To obtain $\psi_a(1)$ from (A13) we must take the limit $Z \rightarrow 1$. For convenience, we continue to use the argument T_{mr}^{\pm} , which is actually $T_{mr}^{\pm}(0, 1)$ in the present case. In letting Z go to unity in (A13) we require the quantity

$$L_1 \equiv \lim_{\epsilon \rightarrow 0} [2 \sum_{s=1}^{\infty} K_0(2\pi s \epsilon) - (2\epsilon)^{-1} - \ln \epsilon], \quad (A17)$$

which is evaluated in Appendix III. The final result for $\psi_a(1)$ is

$$\psi_a(1) = (2z_v e / \epsilon \beta R_1) [M + N], \quad (A18)$$

where

$$M \equiv \gamma_1 + (R_1/4) + \ln [(\alpha/4\pi) \sinh(4\pi/\alpha R_1)]$$

and

$$N \equiv [N(Z) - 2 \sum_{s=1}^{\infty} K_0(T_{00}^-)]_{Z=1},$$

where $N(Z)$ is given in (A15).

We have found that the calculation of $\mathcal{E}_{aic}(X, 0, 1)$ is best carried out by applying the transformations of Appendix I directly to the series

$$\mathcal{E}_{aic}(X, 0, 1) = - \frac{2z_v e}{\epsilon \beta^2 R_1^3} \sum_{l=-\infty}^{\infty} \sum_{m=-\infty}^{\infty} \\ \times \left\{ \left[\left(\frac{X}{R_1} - l \right)^2 + \alpha^2 m^2 + \left(\frac{2}{R_1} \right)^2 \right]^{-1/2} \right. \\ \left. + \left[\left(\frac{X}{R_1} - l - \frac{1}{2} \right)^2 + \alpha^2 \left(m + \frac{1}{2} \right)^2 + \left(\frac{2}{R_1} \right)^2 \right]^{-1/2} \right\}. \quad (A19)$$

Note that since the point of interest is in the IHP, there is no contribution to the normal field from the hexagonal charge array in the IHP and only the image charges contribute to this field. The result of the transformation may be written

$$\begin{aligned} \epsilon_{aic}(X, 0, 1) = & -\frac{4z_0e}{\epsilon\beta^2 R_1^3} \sum_{m=-\infty}^{\infty} \left\{ \left[\left(\frac{2}{R_1} \right)^2 + \alpha^2 m^2 \right]^{-1} + \left[\left(\frac{2}{R_1} \right)^2 + \alpha^2 \left(m + \frac{1}{2} \right)^2 \right]^{-1} \right\} \\ & - \frac{32\pi^2 z_0 e}{\epsilon\beta^2 R_1^3} \sum_{m=-\infty}^{\infty} \sum_{s=1}^{\infty} s^2 \cos \frac{2\pi s X}{R_1} \left[(T_{m0^+})^{-1} K_1(T_{m0^+}) + (-1)^s (T_{m1^+})^{-1} K_1(T_{m1^+}) \right]. \end{aligned} \quad (A20)$$

The single series are summed in Appendix III leading, after simplification, to

$$\begin{aligned} \epsilon_{aic}(X, 0, 1) = & -\frac{4\pi z_0 e}{\epsilon\alpha\beta^2 R_1^2} \coth \frac{4\pi}{\alpha R_1} - \frac{32\pi^2 z_0 e}{\epsilon\beta^2 R_1^3} \\ & \left\{ 2 \sum_{m=1}^{\infty} \sum_{s=1}^{\infty} s^2 \cos \frac{2\pi s X}{R_1} \left[(T_{m0^+})^{-1} K_1(T_{m0^+}) + (-1)^s (T_{m1^+})^{-1} K_1(T_{m1^+}) \right] \right. \\ & \left. + \sum_{s=1}^{\infty} s^2 \cos \frac{2\pi s X}{R_1} \left[(T_{00^+})^{-1} K_1(T_{00^+}) + 2(-1)^s (T_{01^+})^{-1} K_1(T_{01^+}) \right] \right\}. \end{aligned} \quad (A21)$$

This result reduces correctly to $E_{\infty}/2 = -2\pi q_1/\epsilon$ when $R_1 \rightarrow 0$.

APPENDIX III. SUMMATIONS AND LIMITS

$$S_1 \equiv \sum_{p=-\infty}^{\infty} \ln \left[\frac{(p+a)^2 + b^2}{(p+a)^2 + c^2} \right]. \quad (A22)$$

This series, which is involved in Eq. (A9), can be expressed in closed form using the Laplace transform method.²⁸ Since the work necessary is lengthy, a simpler method is to employ the result²⁹:

$$\begin{aligned} \prod_{p=1}^{\infty} \left[\frac{(p+a)^2 + b^2}{(p+a)^2} \right] \left[\frac{(p-a)^2 + b^2}{(p-a)^2} \right] \\ = \frac{\cosh(2\pi b) - \cos(2\pi a)}{2[(a^2 + b^2)/a^2] \sin^2 \pi a} \end{aligned} \quad (A23)$$

in

$$\exp(S_1) = \prod_{p=1}^{\infty} \left[\frac{(p+a)^2 + b^2}{(p+a)^2 + c^2} \right] \left[\frac{(p-a)^2 + b^2}{(p-a)^2 + c^2} \right]. \quad (A24)$$

This leads to

$$S_1 = \ln \left[\frac{(a^2 + c^2)(\cosh(2\pi b) - \cos(2\pi a))}{(a^2 + b^2)(\cosh(2\pi c) - \cos(2\pi a))} \right]. \quad (A25)$$

The quantity L_1 of (A17) may be evaluated by using³⁰

$$\begin{aligned} \sum_{s=1}^{\infty} K_0(2\pi s\epsilon) = & \frac{1}{2} [\gamma_1 + \ln(\frac{1}{2}\epsilon) + (2\epsilon)^{-1}] \\ & + \frac{1}{2} \sum_{l=1}^{\infty} [(\epsilon^2 + l^2)^{-\frac{1}{2}} - l^{-1}]. \end{aligned} \quad (A26)$$

²⁹ I. M. Ryshik and I. S. Gradshteyn, *Tables of Series, Products, and Integrals* (VEB Deutscher Verlag der Wissenschaften, Berlin, 1963), p. 37.

³⁰ Reference 29, p. 335.

The result is

$$L_1 = \gamma_1 - \ln 2 \cong -0.11593152, \quad (A27)$$

where γ_1 is the Euler-Mascheroni constant.

$$S_2 \equiv S_3 + S_4, \quad (A28)$$

$$S_3 \equiv \sum_{m=1}^{\infty} [m^2 + b^2]^{-1}, \quad (A29)$$

$$S_4 \equiv \sum_{m=1}^{\infty} [(m + \frac{1}{2})^2 + b^2]^{-1}. \quad (A30)$$

These series [Eqs. (A28)-(A30)] are involved in Eq. (A20). Series S_3 is well known. Both S_3 and S_4 can be summed using ψ functions. Illustrating this for the unknown S_4 , we find

$$\begin{aligned} S_4 = & (2ib)^{-1} \sum_{m=1}^{\infty} [(m + \frac{1}{2} - ib)^{-1} - (m + \frac{1}{2} + ib)^{-1}] \\ = & (2ib)^{-1} \sum_{m=1}^{\infty} [\psi(\frac{3}{2} + ib) - \psi(\frac{3}{2} - ib)] \\ = & -(b^2 + \frac{1}{4})^{-1} + \pi(2b)^{-1} \tanh(\pi b). \end{aligned} \quad (A31)$$

Since

$$S_3 = -\frac{1}{2} b^{-2} + \pi(2b)^{-1} \coth(\pi b), \quad (A32)$$

$$S_2 = -[(2b^2)^{-1} + (b^2 + \frac{1}{4})^{-1}] + \frac{1}{8} \pi \coth(2\pi b). \quad (A33)$$